SERPENTINITE-WATER INTERACTION AND CHROMIUM(VI) RELEASE IN SPRING WATERS: EXAMPLES FROM TUSCAN OPHIOLITES

Antonio Langone*,°,✉, Ilaria Baneschi*, Chiara Boschi*, Andrea Dini*, Massimo Guidi* and **Andrea Cavallo****

* *Institute of Geosciences and Earth Resources, National Research Council of Italy (CNR), Pisa, Italy.*
° *Institute of Geosciences and Earth Resources, National Research Council of Italy (CNR), Pavia, Italy.*
** *Istituto Nazionale di Geofisica e Vulcanologia (INGV), Roma, Italy.*
✉ *Corresponding author: langone@igg.cnr.it*

Keywords: *Cr(VI) mobility, chromites, serpentinites, hydrochemistry (spring water). Tuscany, Italy*

ABSTRACT

Since 2006 the Regional Environmental Agency (ARPA) of Tuscany has found Cr(VI) concentration in groundwater above the maximum acceptable concentration (5 ppb) according to the Italian regulation (D.M. 25 October 1999, n. 471). Recently, hydrogeological investigations (Grassi, 2009) confirmed high total Cr and Cr(VI) contents in soils and waters related to ultramafic rocks from coastal Tuscany.

To study the release of Cr(VI) to water from geogenic sources we examined the spring waters, soils and bedrocks compositions within two serpentinized bodies of the coastal Tuscany, namely Santa Luce and Querceto. These selected sites are characterized by Cr(VI)-free and Cr(VI)-bearing spring waters, respectively. The prevalence of Mg-HCO_3 waters at these sites indicates that waters are primarily interacting with serpentinites. Samples from Querceto are enriched in Mg suggesting the leaching of brucite. Soil profiles and bedrocks were analysed for major and trace elements by XRF to assess the fate of Cr during weathering. Detailed petrographic and chemical analyses of both soil and rock samples revealed that Cr is mainly hosted within chromites. Chemical data and alteration features indicate a metasomatism coeval to the oceanic serpentinization leading to a Mn-enrichment of the alteration products of primary spinel. The co-occurrence of Mn-bearing and Fe-rich oxides with Cr-rich spinels creates a chemical system potentially able to promote the Cr(III) to Cr(VI) oxidation. However, the occurrence of Mn-rich minerals seems to be not correlated to the oxidation state of chromium in the spring waters. In fact, they are ubiquitous in both the study localities, while Cr(VI) has been detected only at Querceto. Unlike Santa Luce, serpentinites from Querceto contain a significant amount of Fe-rich brucite and show evidence for ongoing brucite dissolution coupled with precipitation of hydromagnesite crusts and veinlets. Formation of complex hydroxy-carbonate minerals could be an alternative way for producing the proper environment for oxidative leaching of chromium from serpentinites to spring waters.

INTRODUCTION

Soils derived from peridotites and serpentinites pose a threat to the surrounding natural environment and adversely affect people's health due to high levels of potentially toxic metals such as Co, Cr, Mn and Ni (e.g., Oze et al., 2004a, 2004b). Although serpentine rocks and soils cover only a small area of the Earth's terrestrial surface, they are abundant in ophiolite belts and have been typically found within regions of the Circum-Pacific margin and Mediterranean Sea (e.g., Oze et al., 2007 and references therein). In these areas, the release of Cr and Ni into the ecosystems during serpentinite weathering suggests that serpentinite landscapes are a possible source of non-anthropogenic metal contamination (e.g., Fantoni et al., 2002; Oze et al., 2004a; 2004b; Garnier et al., 2006; Margiotta et al., 2012; Moraetis et al., 2012).

Chromium is predominantly contained in Cr-bearing spinels (i.e., chromite, Mg-Al-chromite, Al-chromite), which are highly resistant to weathering, and it generally occurs as in the trivalent state resulting not bioavailable (Oze et al., 2004a). It is also found in minor amount in chlorites (e.g., Caillaud et al., 2009), pyroxenes and Fe-oxides and hydroxides (e.g., Gasser et al., 1995). The role of chromite as source of Cr in the environmental processes is still under debate. The chromite resistance to the weathering may favour its accumulation within the soil profile by increasing its abundance (Garnier et al., 2008). Oze et al. (2004a) argued that Cr-spinels are not a significant source of Cr in serpentinite soils, particularly compared to Cr-bearing silicates. Garnier et al. (2008) demonstrated that chromite underwent a chemical modification (i.e., Cr enrichment) during weathering suggesting that chromites are slowly dissolved during pedogenesis. According to these authors, due to the high concentration of chromites in soils and its slow weathering with time, chromites could represent a diffusive minor source of Cr within soils where Cr-bearing silicates remain still a major source.

Independently of the role of chromite as source of Cr, the mobility and availability of Cr to the ecosystems requires oxidation of Cr(III) to Cr(VI). The possible electrons acceptors are Mn-oxides, Fe(III), oxyhydroxides, H_2O_2, dissolved and gaseous O_2 (e.g., Fantoni et al., 2002 and references therein). Mn-oxides are potentially able to rapidly oxidize Cr(III) into Cr(VI) in the environment according to the reaction:

$$Cr(OH)^{2+} + 1.5MnO_2 = HCrO^{4-} + 1.5Mn^{2+}.$$

Cr(III) oxidation by Mn-oxides has already been demonstrated in laboratory studies (e.g., Fendorf, 1995; Oze et al., 2007) but very few have reported evidence for such a reaction in natural systems (Fandeur et al., 2009b and references therein). Recently, Fandeur et al. (2009b) demonstrated by X-ray Absorption Near Edge Structure (XANES) spectroscopy on both bulk natural samples and directly in thin section, the occurrence of Cr(VI) (up to 20% and 33% of total Cr on bulk analyses and on in situ analyses, respectively) in the unit of a regolith which is also enriched in MnO (up to 21.7 wt%). According to these authors, the distribution of Cr(VI) indicates that it is associated to both Mn- and Fe-oxides, with a significant preference for the latter species. Moreover, Fandeur et al., (2009a; 2009b) observed that the largest amounts of Cr(VI) are present in the Fe-oxides located at Mn-oxides boundary suggesting that Cr(VI) could be released from the surface of the Mn-oxides (where it has been oxidized), and subsequently reabsorbed onto the surface of the surrounding Fe-oxides.

Since 2006 the Regional Environmental Agency (ARPA) of Tuscany has found high Cr(VI) concentration, above the maximum acceptable concentration (5 ppb) according to the Italian regulation (D.M. 25 October 1999, n° 471), in groundwater of coastal Tuscany. Recently, hydrogeological investigations (Grassi, 2009) confirmed high total Cr and Cr(VI) content in soil and water related to ultramafic rocks. However, regional investigations on the processes affecting Cr(VI) mobility and promoting its release are absent. RESPIRA, a multidisciplinary research project (FSE-POR 2009-2013) of the Institute of Geosciences and Earth Resources of the National Research Council of Italy (IGG-CNR of Pisa), partially financed by European Union (EU) and Tuscany Region, had among its main aims the study of the release and mobility of Cr within the Critical Zone (NRC, 2001) where rocks (i.e., serpentinites), soils, atmospheric gasses and meteoric waters interact. On the basis of the previous results on similar topic, we organize a further plan of sampling and analysis, in order to select some cases studies to focus on.

This paper illustrates first petrographic and geochemical results obtained from two selected "end-members" sites: Santa Luce quarry and Querceto, characterized by Cr(VI)-free and Cr(VI)-bearing spring waters, respectively. The aim of this work was to put out the potential geochemical processes that can influence metal mobility, distribution, and bioavailability in surficial environments. To achieve this objective, ultramafic rocks, soils and waters were sampled for petrographic and geochemical characteristics and information on (a) mineralogy; (b) textural relations; (c) alterations or changes in the mineralogy; (d) total metal concentrations in the solids and chemical analysis on Cr-bearing minerals; (e) major components and trace metal geochemistry of spring water were discussed.

GEOLOGY AND SITES DESCRIPTION

Tuscany includes the inner part of the Northern Apennines (Fig. 1), that is a Tertiary (Late Cretaceous-Early Miocene) thrust and fold belt resulting from the closure of the Ligurian-Piedmont Ocean (the westernmost portion of the Tethys) and the subsequent collision between the Adria microplate and the European Plate (e.g., Molli, 2008, for a comprehensive review). This process was responsible for the stacking of several tectonic units derived from the oceanic Ligurian Domain (Jurassic-Eocene), the epi-continental Subligurian Domain (Cretaceous-Oligocene) and the continental Tuscan Domain (Palaeozoic-Early Miocene). Tectonic units derived by the oceanic Ligurian Domain represent the uppermost nappes of the Apennine stack, overlying a complex pile of Subligurian and Tuscan tectonic units.

Ligurian units can be subdivided on the basis of stratigraphic and structural features into two main groups (Fig 1; Elter, 1975): (i) the Internal Ligurian Units which are characterized by an ophiolite basement (serpentinite, gabbro and basalt) and a Late Jurassic to Early Cretaceous sedimentary cover (Marroni and Pandolfi, 1996); (ii) the External Ligurian Units mainly consisting of calcareous-marly turbiditic units (Cretaceous-Paleocene; Helminthoid Flysch) locally embedding ophiolite olistoliths and ophiolite-derived debris (Marroni et al., 1988). The main Tuscan ophiolite outcrops belong to the Internal Ligurian Units (Nirta et al., 2005).

The two case study sites, Santa Luce and Querceto, are located in central western Tuscany being hosted by two of the most important ophiolitic outcrops of the Internal Ligurian Units (Fig. 1). Santa Luce quarry exploited the northwestern margin of a large serpentinite body, associated with minor basalts and gabbros, forming an east-west elongated relief. The sedimentary envelope is constituted by shales and limestones cropping out north-east of the quarry, while

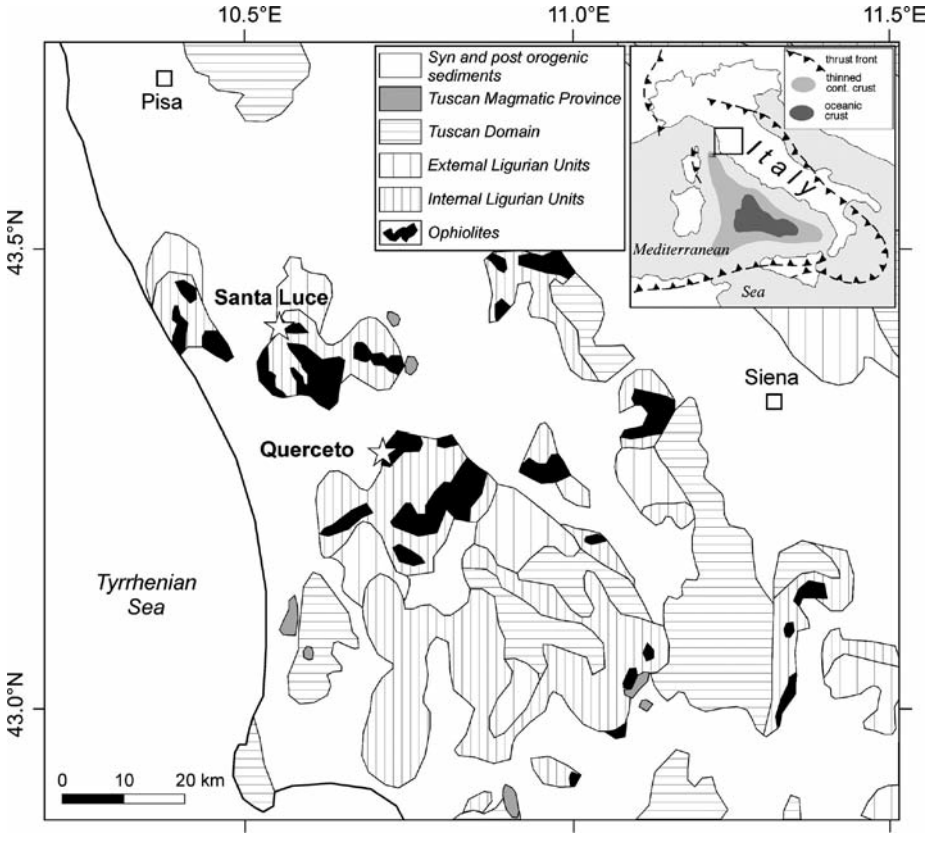

Fig. 1 - Geological sketch map of Southern Tuscany showing the distribution of ophiolites and sample locations (stars).

to the west, serpentinites are covered by Neogene sediments. The quarry (ca. 300 x 150 m, with a vertical height of 50 m) is entirely excavated in massive serpentinites (Fig. 2a) locally crosscut by plagiogranite dykes. Fractures are very frequent but only the lowermost central area of the quarry is characterized by a discontinuous, low-outflow spring. The Querceto site (q. 300 m a.s.l.) is located in a small creek on the southwestern flank of Monte Aneo (q. 520 m), at the western end of a large body of serpentinite embedded in shales. The presence of water outflow was investigated in the past by construction of a spring water captation consisting of a short drainage tunnel (Fig. 2b). The drainage tunnel is still accessible allowing observation and sampling of the relatively constant low-outflow spring.

Typically ultramafic (serpentine) soils are shallow, well drained and prone to erosion, with typical serpentine vegetation consisting of garigues (chamaephytic and annual plants on shallow or rocky soils) and grasslands (Chiarucci et al., 1995). The soils in the study sites are classified both as Lithic Ustorthents loamy-skeletal, mixed, nonacid, mesic (MGA1, sit.lamma.rete.toscana.it/websuoli/doc/legendone.pdf, Soil Survey Staff, 2003 - USDA) or Chromic Cambisol (F.A.O., 1998).

Soils are poorly developed in Santa Luce quarry; the intrinsic low fertility of serpentinitic soils (e.g., Chiarucci et al., 2003) does not allow the development of a thick vegetation cover, and the relatively steep slopes limit pedogenic processes. The vegetation is discontinuous, characterized by low ground cover of garigue with patches of stunted plants belonging to the Viburno - Quercetum ilicis and several endemic species (like nickel-hyperaccumulator *Alyssum bertolonii*), associated with an area where bare rock crops out (Perugi et al., 1995; Chiarucci et al., 1995). In Querceto, the vegetation is characterized by the sparsely distributed and introduced pines, with typical serpentine vegetation restricted to open patches and slopes, higher evergreen shrub.

The aquifers in the study area of Santa Luce consist of serpentinites, conglomerates, limestones and marlstones, and the springs are generally located in the contact with lower-permeability terrains or along fractures. Instead, in the Querceto site, groundwaters are hosted mainly in serpentinite aquifers. The SLW-1 spring in Santa Luce quarry

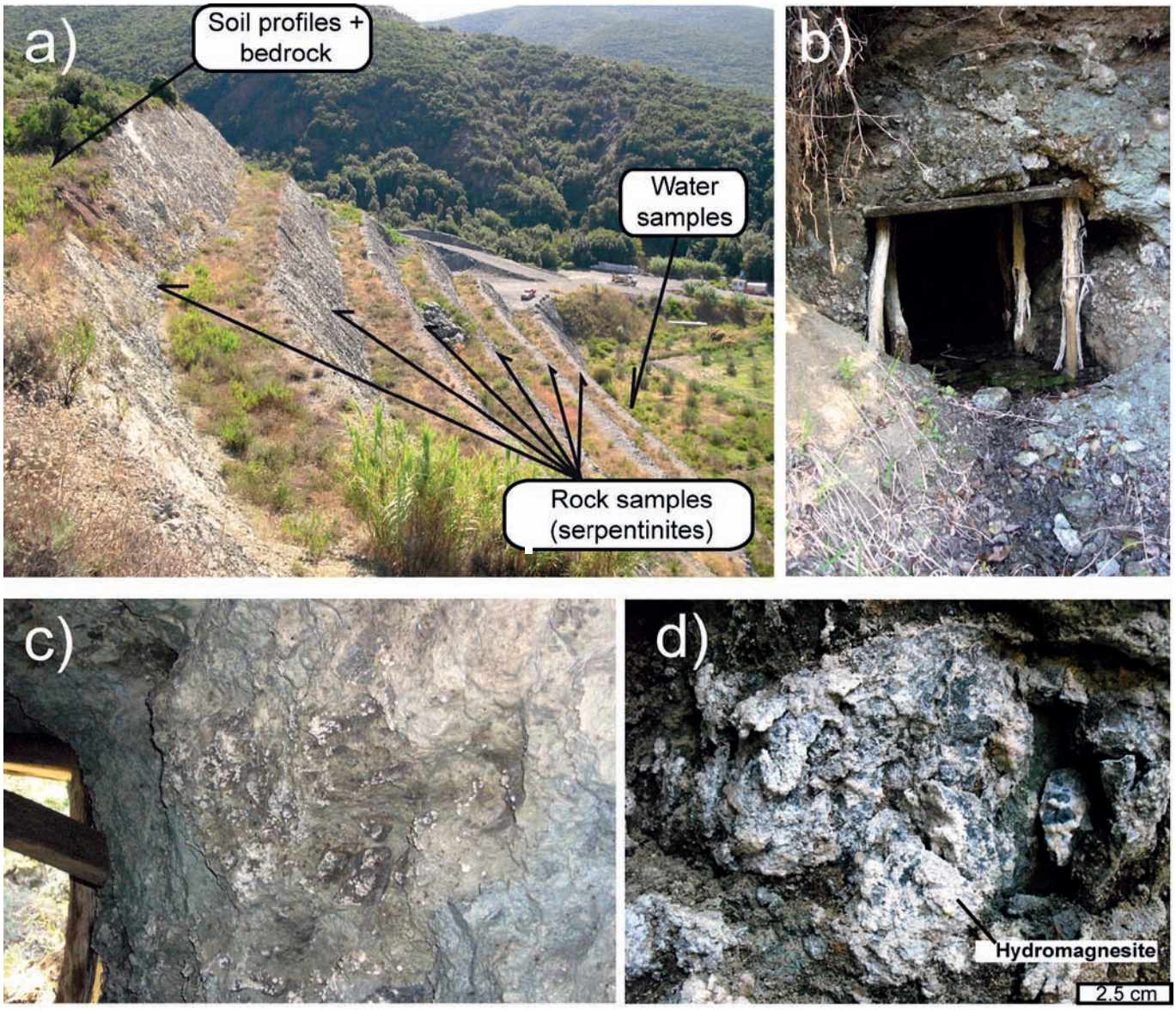

Fig. 2 - Photos of Santa Luce quarry (a) and Querceto (b-d). a) Photo of the Santa Luce quarry showing samples locations. b) Photo of the entrance of the drainage tunnel in Querceto. c) Photo from the interior of the drainage tunnel showing hydromagnesite precipitations on the walls. d) Detail of c).

is quite superficial and with a discontinuous flow rate, whereas the QUW-1 spring in Querceto is characterized by a relatively continuous flow rate.

The climate of the two areas is hot-summer Mediterranean-type (Csa, sensu Koppen, 1936) with hot and dry summers and mild, wet winters. Santa Luce (about 190 m a.s.l.) has mean yearly rainfall of 800 mm, with November being the rainiest month (about 130 mm), July the driest (about 20 mm). The mean monthly temperature ranges between 3.7°C (January) and 31°C (August). The mean yearly rainfall at Querceto (240 m a.s.l.) is 810 mm, with a peak on November (125 mm) and a minimum on July (10 mm). The mean annual temperature is 14.8°C, the average temperature of the coldest month is 4°C (February) and the average temperature of the warmest month (August) is 29°C.

SAMPLING

After preliminary fieldwork and chemical analyses of spring waters, Santa Luce and Querceto sites were selected based on the different content of total Cr and Cr(VI). In addition, the locations are quite easily accessible and well representative of the serpentinite outcrop with water emergencies. In both localities, bedrock, soil and water were sampled.

Waters emerging directly from serpentinites were collected for chemical and physic-chemical analyses. At the Santa Luce quarry the spring water was collected on September 2010, March 2011 and 2012, May 2011 and July 2011. The spring water in Querceto was sampled twice on March 2011 and April 2012.

At Santa Luce site, serpentinized harburgites have been sampled from the quarry front, at different levels (Fig. 2a). The rocks are deeply serpentinized, with well-developed retrograde pseudomorphic mesh textures, and late veining of white fibrous serpentine, of most probably chrysotile composition. Serpentinite samples have been collected also directly from the base of the soil profiles (soil bedrock: SLSM-1; SL-1D). The SL-5 sample has been collected near the spring water. At Querceto, a serpentinite sample (QU-2) has been collected within the drainage tunnel (Fig. 2b), close to the spring water outflow. The walls of the cave are locally covered by white globular precipitations of probably hydrated Mg-carbonate composition (Fig. 2c, d), which have been sampled as separates together with the serpentinitic substrate (QU-3); in addition, clay-rich alteration products, at the base of the spring water, have been collected (QU-clay).

Soil profiles were sampled at the two sites with the related ultramafic bedrock. A pit was opened at the top of the Santa Luce quarry until stones predominated (soil horizon samples: SLS-1A, B, C). The soil horizons from the Querceto site were sampled from an exposed soil profile at the top of the spring water (soil horizon samples: QUS-A, B, C).

ANALYTICAL METHODS

Water samples were physically and chemically characterized in the field (with portable instruments) and at the IGG-CNR laboratories of Pisa. Rock and soil samples from both localities were characterized using optical microscope, Field Emission-Scanning Electron Microscope (FE-SEM), Electron microprobe (EMPA) and X-Ray Fluorescence (XRF).

Temperature, pH and conductivity of each water sample was measured in the field by a portable instrument (HD2156.2, DELTA OHM), calibrated in laboratory before sampling. Total alkalinity was also determined in the field by acidimetric titration, using HCl 0.1 N as titrating agent and methyl orange as indicator. At each site, a sample was collected in new polyethylene (PE) bottles, filled to the top and capped without leaving any head space, for anions and Silica analyses. Samples for cations (Ca, Mg, Na and K) and trace elements (total Cr, Ni, Fe, Mn) were filtered through 0.45 m Acetate-cellulose membrane filters in the field, acidified with Suprapur® HNO_3 (2% v/v) in order to prevent metal precipitation, and stored in PE- bottles (50 ml) previously acid washed with diluted HNO_3, rinsed with deionized water in laboratory and rinsed three time with small amounts of sample. Cr(VI) separations were performed directly in the field using a cation-exchange cartridge (IC-H, Alltech) which allows separating (speciation) Cr(VI) and Cr(III) forms (Ball and McCleskey, 2003). Sample (2 ml) was forced, at no more than two drops per second, through an acetate-cellulose membrane syringe filter and the cation-exchange cartridge into a PE-bottle (10 ml). The sample issuing from the cartridge contains only Cr(VI), directly measured as Cr (total) in laboratory by Inductively Coupled Plasma Optical Emission Spectrometer (ICP-OES Optima 2000, Perkin Elmer). In the laboratory, the concentrations of anions were determined by using a Dionex 100 Ion chromatograph. Cations and trace metals were analysed by ICP-OES. Silica was determined by means of the spectrophotometric method (β-silico-molybdenum blue). Thermodynamic calculations were performed using geochemical modelling program Visual MINTEQ with the thermodynamic database of MINTEQA2. The pCO_2 was calculated using field pH and alkalinity, and chemical composition as inputs for Visual MINTEQ software.

Major and trace elements analyses of whole rocks and soil samples were performed at the Dipartimento di Scienze della Terra of the Pisa University by XRF using a Philips PW 1450 spectrometer on powder pellets obtained mixing 5-6 g of sample powders with 0.5 ml of binder (a 20% aqueous solution of polyvinylic alcohol). The mixture, finely grounded, was dried further at 110°C overnight and then pressed into sample holder on a boric acid base. Component concentrations were determined according to Franzini et al. (1975) and Leoni and Saitta (1976), using adequate international standards of rocks and minerals. Loss on ignition (L.O.I.) was determined by the gravimetric method after heating samples at 950°C for 4 hours.

The soil samples were air-dried, cleaned (hand picking) for the organic matter and sieved to less than 2 mm prior to the chemical analysis and petrographic observations. Moreover, for the petrographic analyses at the FE-SEM and EMPA the different horizons of the two profiles have been further subdivided in five fractions: > 2 mm; $2 \text{ mm} > f > 0.50$ mm; $0.50 \text{ mm} > f > 0.25$ mm; $0.25 \text{ mm} > f > 0.10$ mm; $0.10 \text{ mm} > f > 0.04$ mm.

The mineral characterization has been performed on both polished mounts of soil separates and on ordinary thin sections of rocks. Samples have been studied preliminarily by acquiring Back Scattered Electrons (BSE) images at the National Institute of Geophysics and Volcanology (INGV) of Rome, by using a Jeol JSM-6500F thermal Field emission scanning microscopy (FE-SEM).

Major element mineral composition was determined at the Dipartimento di Scienze della Terra of the Milano University and at the CAMPARIS Service of the Paris 6/7 Uni-

versity using a JEOL JXA 8200 Superprobe and Cameca microprobes (SX100 and SXFive), respectively. Operating conditions were 1-3 μm beam diameter, 15 kV accelerating voltage, and 15 nA beam current. Natural and synthetic minerals and glasses were used as standards. All standards were calibrated within 0·5% at one standard deviation. Raw data were corrected using a Phi-Rho-Z quantitative analysis program. Abbreviations for minerals in figures and tables are according to Whitney and Evans (2010).

RESULTS

Water chemistry

The average temperature, alkalinity and pH of the collected spring waters are reported in Table 1. Heavy metals (Cr, Fe, Mn, Ni) concentrations are reported in Table 2.

In the triangular plot involving the three major anions (Fig. 3a) all samples fall into HCO_3 field, indicating that the chemistry of local shallow ground waters are chiefly dominated by the serpentinite-water interaction (Garrels, 1968).

In the triangular diagram involving the four major cations (Fig. 3b), all the waters interacting with serpentinites are situated in the Mg field, indicating that their Mg-HCO_3 chemical composition resulted from the interaction with ultramafic rocks affected by serpentinization (e.g., Bruni et al., 2002; Fantoni et al., 2002; Cipolli et al., 2004). Differently, SLW-S1, SLW-S2, SLW-S3 and SLW-S4 waters are in the Ca field, indicating a Ca-HCO_3 composition where Ca is controlled by the dissolution of Ca-rich phases. Moreover, in the Mg vs Ca plot (Fig. 3c) the Ca-HCO_3 and Mg-HCO_3 waters form distinct group. The Mg-HCO_3 waters are characterized by Ca/Mg molar ratio below 0.25, whereas for Ca-HCO_3 waters Ca/Mg ratio ranges from 12 to 18.

The Santa Luce springwater (SLW-1) is very shallow with a discharge quite low and variable. It was sampled several times to analyse the chemical variability during dry (summer) and wet (spring) season. For all the samples SLW-1 hydrochemical facies does not change (Mg-HCO_3), even if the concentrations of major ions vary relatively, reflecting mainly the discharge changes.

The pCO_2 of Mg-HCO_3 waters in Santa Luce range from 8.23E-3 to 1.75E-3 atm, whereas pCO_2 of Ca-HCO_3 waters range from 5.07E-2 to 1.05E-1 atm. In Querceto, the pCO_2 ranges from 5.17E-3 to 1.23E-2 atm. These reflect the fact that Mg-HCO_3 waters derived from the dissolution of serpentinites, which produce enrichment in Mg.

The triangular plot Mg-SiO_2-HCO_3 (Fig. 3d) is useful to investigate qualitatively the water rock interaction processes affecting Mg-HCO_3 waters (Fantoni et al., 2002). It reports also the expected composition of aqueous phases produced by CO_2-driven dissolution of Mg-bearing rocks assuming congruent dissolution. The Ca-HCO_3 and Mg-HCO_3 waters are well distinguished, with Ca waters pointing toward the HCO_3 apex. Moreover, the HCO_3/Mg molar ratio of all the Mg-HCO_3 waters is close to 2, that is the theoretical value expected for Mg-bearing solid phase (constrained electronically), and plot to the left to the serpentine point. This indicates that Mg-HCO_3 waters originated from incongruent dissolution of serpentine together with precipitation of phases rich in SiO_2. In particular the waters from Santa Luce plot near serpentine point more than waters from Querceto, which are closer to Mg-carbonates/hydroxides point.

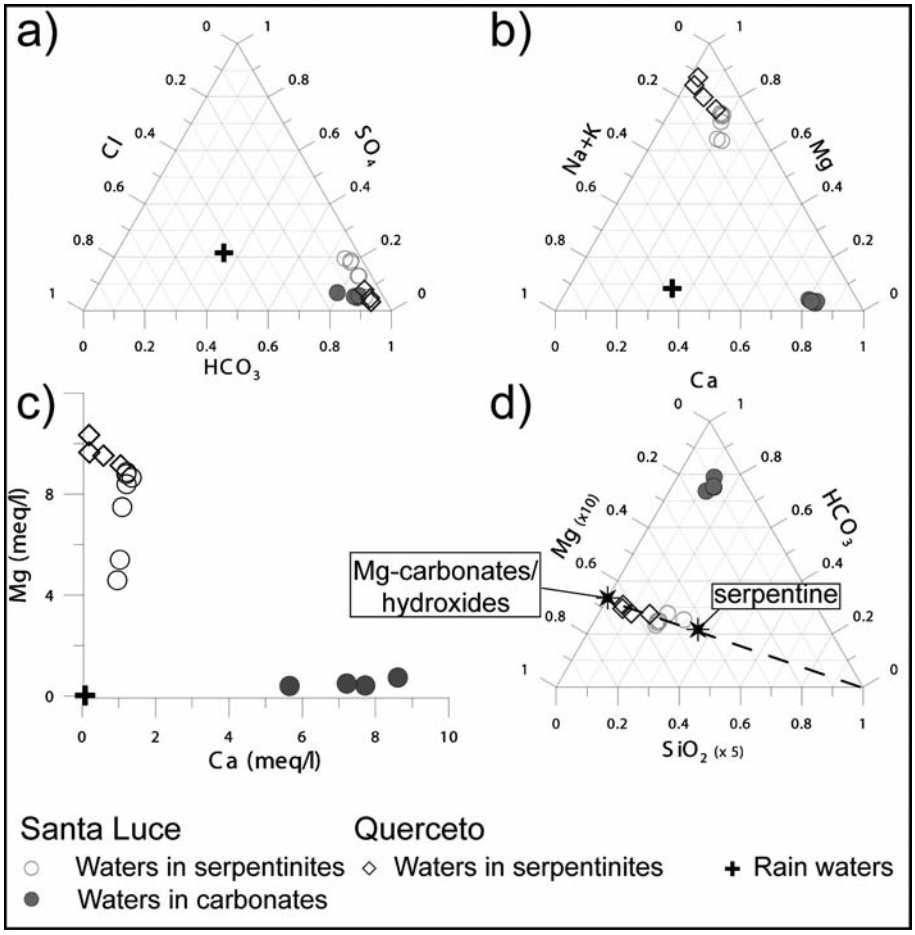

Fig. 3 - Major ion chemistry of water samples. Rainwater composition represents mean values reported for two Tuscan rain-stations of the CONECOFOR project (Marchetto et al., 2012). a) HCO_3-SO_4-Cl triangular plot and b) Ca-Mg-(Na-K) triangular plot for the waters of the study area, computed from concentration in mg/L. c) Mg vs. Ca for water samples. d) Mg-SiO_2-HCO_3 triangular plot computed from concentration in mg/l. Stars represent the expected compositions of aqueous phase controlled by CO_2-driven dissolution of Mg-bearing solid phases.

Table 1 - Chemical and physical characteristics of water samples.

Sample	Date	Lithology	T (°C)	pH	Cond (µS/cm)	Alk (mmol/l)	Ca (mg/l)	Mg (mg/l)	K (mg/l)	Na (mg/l)	Cl (mg/l)	SO_4 (mg/l)	SiO_2 (mg/l)
SLW-1	16/09/2010	Serpentinites	29.0	8.30	893	7.3	27.0	103.8	2.70	13.3	31.9	115.4	
SLW-1	11/03/2011	Serpentinites	13.7	8.04	605	6.1	21.9	89.8	0.30	10.6	18.0	90.5	66.7
SLW-1	13/05/2011	Serpentinites	20.0	8.36	801	7.9	24.1	105.5	0.19	13.0	23.7	75.2	80.1
SLW-1	12/07/2011	Serpentinites	31.0	8.24	1031	8.0	24.3	106.4	0.16	13.8	25.9	76.9	83.3
SLW-1	23/03/2012	Serpentinites	16.2	8.08	710	7.3	24.2	100.7	0.28	13.1	24.2	103.0	75.6
SLW-S1	19/03/2011	Calcareous-marly Flysch	13.2	6.54	903	7.5	172.1	8.9	1.37	32.2	82.4	38.9	14.9
SLW-S2	19/03/2011	Calcareous-marly Flysch	12.6	6.86	745	7.3	154.3	5.1	0.85	25.8	44.9	25.0	13.5
SLW-S3	19/03/2011	Calcareous-marly Flysch	12.3	6.81	709	6.7	144.3	6.0	0.98	22.3	45.6	25.4	15.1
SLW-S4	19/03/2011	Calcareous-marly Flysch	10.9	7.07	546	5.5	113.1	4.9	1.07	20.0	30.0	21.9	12.0
SLW-S5	24/03/2011	Serpentinites	17.0	7.57	602	5.9	20.6	64.8	0.48	14.9	24.2	21.0	58.2
SLW-S7	24/03/2011	Serpentinites	10.6	7.55	435	5.0	19.2	55.1	0.42	11.8	16.2	13.6	69.7
QUW-1	06/04/2011	Serpentinites	14.7	8.05	760	9.4	3.8	124.0	0.97	13.3	31.8	20.5	26.7
QUW-1	27/03/2012	Serpentinites	14.4	7.94	707	9.3	4.0	115.8	1.00	16.4	30.8	20.4	23.3
QUW-2	06/04/2011	Serpentinites	13.7	7.52	715	8.4	11.7	114.2	0.28	16.8	28.8	46.0	39.1
QUW-3	06/04/2011	Serpentinites	13.0	7.36	720	8.8	21.0	109.6	0.58	14.2	27.2	27.8	65.8

Prefixes SLW and QUW refer to samples from Santa Luce and Querceto sites, respectively.

Table 2 - Heavy metals (Cr, Fe, Mn, Ni) concentrations of water samples.

Code	Date	Lithology	Cr (Tot) (µg/L)	Cr VI (µg/L)	Cr III (µg/L)	Fe (µg/L)	Mn (µg/L)	Ni (µg/L)
SLW-1	16/09/2010	Serpentinites	n.d.	n.d.	n.d.	n.d.	n.d.	n.d.
SLW-1	11/03/2011	Serpentinites	4.1	< 0.1	4.1	< 1	< 1	28
SLW-1	13/05/2011	Serpentinites	5.0	< 0.1	5.0	< 1	< 1	39.0
SLW-1	12/07/2011	Serpentinites	4.2	< 0.1	4.2	< 1	< 1	31.6
SLW-1	23/03/2012	Serpentinites	4.3	< 0.1	4.3	11	< 1	36.7
SLW-S1	19/03/2011	Calcareous-marly Flysch	< 0.1	< 0.1	< 0.1	9	2	< 0.1
SLW-S2	19/03/2011	Calcareous-marly Flysch	< 0.1	< 0.1	< 0.1	< 1	< 1	< 0.1
SLW-S3	19/03/2011	Calcareous-marly Flysch	< 0.1	n.d.	< 0.1	< 1	< 1	< 0.1
SLW-S4	19/03/2011	Calcareous-marly Flysch	< 0.1	< 0.1	< 0.1	< 1	4	< 0.1
SLW-S5	24/03/2011	Serpentinites	6.5	< 0.1	6.5	< 1	< 1	2.7
SLW-S7	24/03/2011	Serpentinites	4.8	n.d.	n.d.	< 1	< 1	14
QUW-1	06/04/2011	Serpentinites	55.0	48.9	6.1	< 1	< 1	3.1
QUW-1	27/03/2012	Serpentinites	44.4	44.0	< 0.1	24	< 1	2.0
QUW-2	06/04/2011	Serpentinites	14.0	< 0.1	14.0	< 1	2	13
QUW-3	06/04/2011	Serpentinites	6.3	n.d.	n.d.	14	< 1	34

Prefixes SLW and QUW refer to samples from Santa Luce and Querceto sites, respectively.

Table 3 - XRF chemical data (major elements and V, Cr, Co and Ni) of serpentinitic samples from Santa Luce and Querceto.

Locality	Santa Luce quarry				Querceto		*av.VC
Name	SLSM-1[a]	SL-1D	SL-3	SL-5	QU-2[a]	QU-clay[b]	
(wt%)							
SiO_2	40.66	42.60	42.75	42.41	39.50	42.90	39.54
TiO_2	0.06	0.06	0.04	0.04	0.04	0.00	0.06
Al_2O_3	2.28	2.77	2.20	1.58	1.63	0.68	1.31
Fe_2O_3	8.50	7.11	5.63	5.60	8.27	6.14	4.24
FeO							2.58
MnO	0.10	0.10	0.09	0.10	0.09	0.07	0.11
MgO	33.78	33.63	35.90	37.08	37.30	37.75	39.32
CaO	0.81	1.31	1.06	0.08	0.04	0.05	0.66
Na_2O	0.00	0.00	0.00	0.00	0.00	0.00	0.08
K_2O	0.01	0.02	0.01	0.01	0.01	0.01	n.rep.
P_2O_5	0.00	0.02	0.01	0.00	0.00	0.00	0.00
L.O.I.	13.80	12.40	12.30	13.10	13.13	12.40	12.10
(ppm)							
V	51	57	53	47	55	15	59
Cr	3118	2630	2550	2710	2534	1499	2383
Co	112	119	124	130	141	162	101
Ni	2583	1976	1928	1907	2584	2716	2274

([a]) serpentinitic bedrock directly below the soil profiles; ([b]) clay-rich alteration product of serpentinites. The average composition of serpentinites from Val di Cecina (Mellini et al. 2005) are also reported. L.O.I.- Loss on Ignition.

Table 4 - XRF chemical data (major elements and V, Cr, Co and Ni) of soil horizons from Santa Luce (SLS) and Querceto (QUS) profiles.

Location	Santa Luce quarry			Querceto		
Horizon	SLS-1A	SLS-1B	SLS-1C	QUS-A	QUS-B	QUS-C
(wt%)						
SiO_2	37.48	41.87	40.50	42.35	44.30	38.99
TiO_2	0.21	0.31	0.21	0.03	0.00	0.00
Al_2O_3	5.10	6.95	5.72	1.72	0.57	0.50
Fe_2O_3	7.26	8.67	11.15	8.95	8.07	8.26
MnO	0.13	0.18	0.16	0.12	0.11	0.11
MgO	25.87	24.21	25.66	32.76	33.40	36.09
CaO	1.95	1.69	1.33	0.39	0.07	0.10
Na_2O	0.43	0.46	0.12	0.00	0.00	0.00
K_2O	0.22	0.33	0.23	0.09	0.01	0.00
P_2O_5	0.04	0.04	0.03	0.00	0.00	0.00
L.O.I.	21.30	15.30	14.90	13.58	13.47	15.94
(ppm)						
V	71	93	84	25	14	11
Cr	2765	3099	3196	1985	1514	1702
Co	96	131	123	157	141	139
Ni	1454	1701	2192	2923	2394	2529

L.O.I.- Loss on Ignition.

Total Cr concentrations in Santa Luce are generally low. In particular, Cr contents were below the detection limit (0.1 g/L) in Ca-HCO_3 waters, whereas in Mg-HCO_3 waters the mean value is 4.9 ± 0.8 g/L essentially in the trivalent form. Differently, in Querceto the Cr concentration found in QUW is near the maximum admissible concentration (MAC) of 50 g/L defined by Italian legislation (DL 152/2006) and occurs primarily in the hexavalent form exceeding the MAC of 5 g/L (mean value of 49.5 g/L), indicating an oxidant system. The dissolved Ni concentrations are below the detection limit for Ca-HCO_3 waters, whereas in Mg-HCO_3 waters the mean value is 29.6 and 13.0 g/L in Santa Luce and Querceto, respectively. Correlation of Ni with Cr-species is not significant. Among the other trace metals, concentrations are generally low and even below the detection limit, also for dissolved total Fe and Mn concentration in Ca and Mg-HCO_3 waters, as expected considering the pH of the waters and the oxidizing environment.

Bedrock petrography and composition

Santa Luce spinel harzburgites underwent a deeply serpentinization, even if few relicts of the primary mineral assemblage are still recognisable (Fig. 4a). In particular, few clinopyroxene relicts are mostly unaffected by serpentinization process, whereas spinel crystals are preserved with variable degree of alteration; by contrast, olivine and orthopyroxene relicts have been observed only in one sample. Serpentine replacement develops from the rims of primary minerals or along the pyroxene cleavage. Olivines have been almost totally altered in mesh-textured serpentine, whereas orthopyroxenes show the typical alteration to pseudomorphic serpentine bastite.

Primary Mg-Al-spinels are variable in size (from few microns up to 2.5 mm), show lobate shape typical of spinels included in mantle rocks. Their alteration features reflect the degree of serpentinization (Fig. 4b): Mg-Al-spinels are fully transformed into variable amount of secondary Fe-rich spinel and Mg-rich silicates, when serpentinization is complete. Under optical microscope, they appear orange to deep red with a variable thick opaque rim (Fig. 4a), recalling the highly reflective Fe-chromite rims around chromites (e.g., Mellini et al., 2005). According to the BSE images acquired at the FE-SEM, spinel alteration is highlighted by a marked difference in brightness, indicating chemical zoning from primary composition (dark grey, Mg-Al-spinel) to variable Fe-enriched domains (light grey to white, Fe-chromite to magnetite). Most of the time, they show a dark domain (i.e., primary chemical composition), surrounded by increasingly brighter (i.e, increasingly iron-enriched) outer domain (Fig. 4b). Where the primary spinel is poorly affected by alteration, thin and discontinuous rims of Fe-chromite are present. With a major degree of alteration, Fe-chromite is also present along fractures. Generally, spinels totally altered are characterized by domains consisting of very fine-grained aggregates of silicates and oxides. The brightness of these domains is related to the relative proportion of silicates (dark grey) and oxides (light grey to white). Also in this case, Fe-chromite forms discontinuous rims. Fe-chromite and the fine-grained aggregates of silicates and oxides clearly grow at the expense of the primary chromite: alteration products and relict of the primary chromite together define the shape of the original chromite crystal (Fig. 4b). Very bright (white) thin rims of magnetite occur independently of the degree of alteration. Magnetite may also be present along fractures together with Fe-chromite. Porosity commonly occurs on the altered domains.

Secondary magnetite, produced during serpentinization, occurs generally in mesh-textured rims with serpentine or along the inner parting of the mesh rims. In one sample, late anhedral crystals of Ca-rich hydrogarnet and fibrous tremolite have been observed along bastite boundary, suggesting Ca metasomatism. Finally, late serpentine veins cut the pseudomorphic textures.

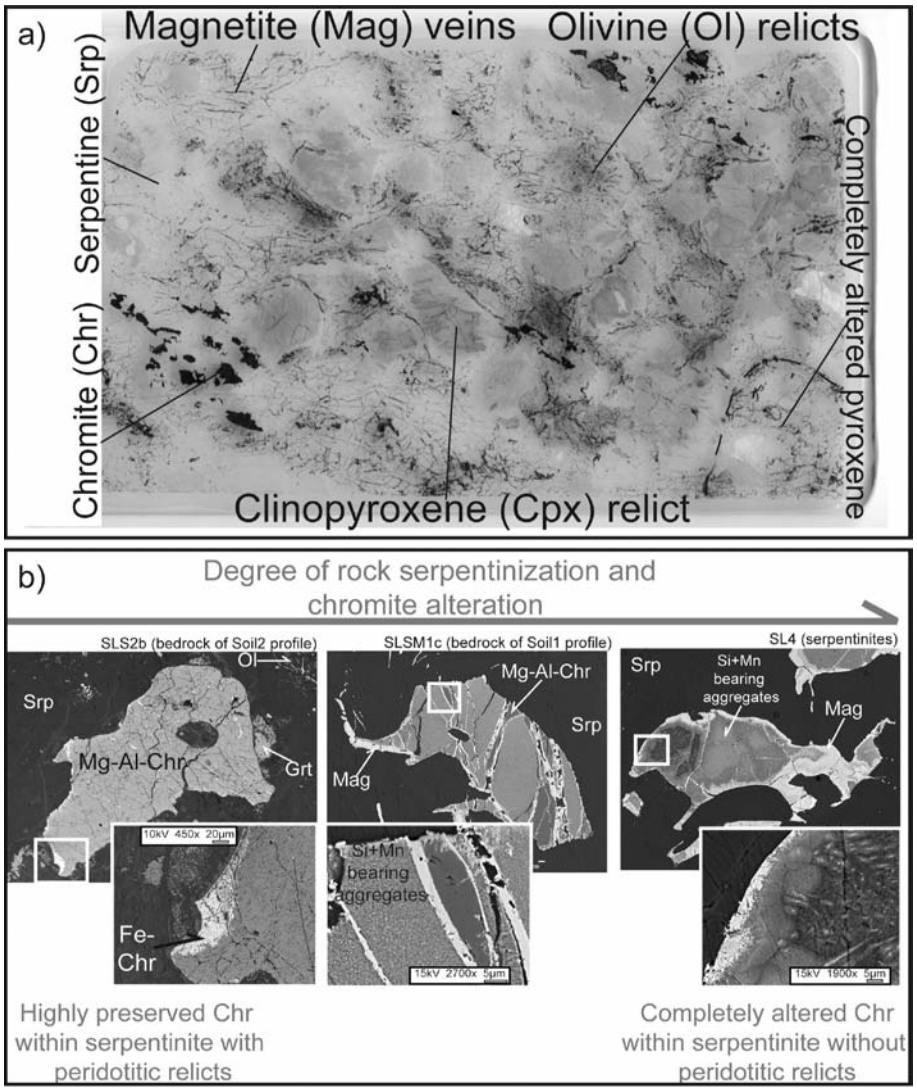

Fig. 4 - Petrographic features of serpentinite rock samples from Santa Luce quarry. a) Scan of a serpentinite thin section showing main textural features and mineralogy. b) FE-SEM BSE images of chromite showing different degree of alteration.

Table 5 - Average chemical composition of serpentine, garnet, chlorite, chromite and magnetite from rock and soil (grey filled columns) samples of the Santa Luce quarry.

Mineral	Serpentine		Garnet			Chlorite	Chromite		Magnetite	
			Adr	H-Grs						
(wt.%)										
SiO_2	40.48 *[35.85-44.88]*	41.62 *[34.83-45.43]*	35.69	36.79	33.69 *[31.24-37.23]*	32.91 *[29.48-34.83]*	0.04 *[0.00-0.13]*	0.08 *[0.06-0.09]*	1.46 *[0.19-5.58]*	0.91 *[0.11-2.87]*
TiO_2	0.07 *[0.00-0.34]*	0.04 *[0.00-0.40]*	0.03	0.05	1.56 *[0.00-5.62]*	0.02 *[0.00-0.07]*	0.54 *[0.35-0.88]*	0.19 *[0.00-0.42]*	0.05 *[0.00-0.17]*	0.09 *[0.00-0.23]*
Al_2O_3	1.86 *[0.11-5.98]*	1.58 *[0.08-6.20]*	2.90	21.58	0.85 *[0.29-1.73]*	12.17 *[6.20-14.46]*	27.82 *[1.42-34.37]*	36.72 *[25.85-43.15]*	0.04 *[0.00-0.09]*	0.14 *[0.00-1.04]*
Cr_2O_3	0.37 *[0.00-1.28]*	0.29 *[0.00-1.70]*	0.00	0.02	0.24 *[0.00-1.00]*	1.08 *[0.66-1.35]*	31.57 *[26.29-34.12]*	29.46 *[22.89-41.23]*	0.13 *[0.01-0.44]*	0.75 *[0.00-3.24]*
FeO	5.47 *[2.13-9.76]*	4.23 *[2.12-7.50]*	23.91	0.57	25.69 *[21.52-27.78]*	4.43 *[3.66-5.39]*	23.64 *[16.56-56.41]*	19.65 *[15.63-23.72]*	88.46 *[81.51-91.58]*	88.24 *[81.06-94.08]*
MnO	0.10 *[0.00-0.24]*	0.09 *[0.00-0.65]*	0.09	0.55	0.06 *[0.02-0.09]*	0.04 *[0.00-0.08]*	1.13 *[0.01-7.28]*	0.19 *[0.13-0.26]*	0.11 *[0.05-0.19]*	0.21 *[0.03-0.64]*
MgO	32.78 *[26.33-39.28]*	36.54 *[29.41-40.97]*	0.08	0.07	0.44 *[0.02-1.14]*	31.92 *[26.99-37.65]*	13.14 *[1.07-15.70]*	14.79 *[13.37-17.33]*	1.72 *[0.24-6.70]*	1.13 *[0.37-2.10]*
CaO	0.16 [0.00-0.39]	0.10 [0.02-1.06]	32.94	36.08	33.06 [31.83-33.57]	0.07 [0.00-0.24]	0.02 [0.00-0.08]	0.03 [0.01-0.08]	0.04 [0.01-0.05]	0.05 [0.00-0.21]
NiO	0.48 *[0.09-1.21]*	0.19 *[0.06-0.38]*					0.18 *[0.11-0.31]*	0.15 *[0.14-0.16]*	0.11 *[0.02-0.22]*	0.22 *[0.00-0.72]*
	n=21	n=26	n=1	n=1	n=9	n=8	n=7	n=3	n=5	n=14

n- number of analyses; [a-b]- concentration range; H-Grs- hydro-grossular.

Table 6 - Average chemical composition of serpentine, garnet, chlorite, chromite, magnetite and brucite from rock and soil (grey filled columns) samples of the Querceto site.

Mineral	Serpentine		Garnet	Chlorite	Chromite		Magnetite		Brucite* Fe-rich	
(wt.%)										
SiO_2	37.10 *[31.55-40.09]*	39.92 *[31.15-44.21]*	32.46 *[26.45-40.14]*	34.28 *[29.36-37.58]*	1.40 *[0.47-2.67]*	1.14 *[0.05-3.45]*	0.77 *[0.52-0.89]*	0.59 *[0.21-1.39]*	1.17 *[0.85-1.51]*	0.91 *[0.54-1.28]*
TiO_2	0.02 *[0.00-0.07]*	0.02 *[0.00-0.09]*	0.23 *[0.06-0.49]*	0.01 *[0.00-0.03]*	0.55 *[0.43-0.69]*	0.42 *[0.09-0.84]*	0.02 *[0.02-0.03]*	0.08 *[0.00-0.28]*	0.07 *[0.00-0.22]*	0.00
Al_2O_3	0.53 *[0.24-1.58]*	1.22 *[0.20-5.09]*	3.02 *[2.02-7.04]*	7.64 *[2.28-19.82]*	0.92 *[0.51-1.27]*	10.37 *[0.44-35.76]*	0.01 *[0.00-004]*	0.12 *[0.00-0.87]*	0.00	0.00
Cr_2O_3	0.38 *[0.00-1.48]*	0.39 *[0.00-3.15]*	0.37 *[0.00-1.03]*	3.14 *[0.57-7.60]*	33.84 *[30.04-37.47]*	33.45 *[23.36-44.63]*	0.02 *[0.00-0.09]*	1.99 *[0.00-7.14]*	0.20 *[0.00-0.36]*	0.16 *[0.11-0.21]*
FeO	4.08 *[2.55-5.10]*	4.54 *[2.36-8.92]*	22.21 *[9.86-24.42]*	4.02 *[2.24-6.71]*	47.82 *[43.50-52.95]*	41.63 *19.50-66.82]*	86.26 *[85.14-87.92]*	87.86 *[76.13-92.61]*	32.59 *[27.74-35.25]*	13.45 *[12.90-14.00]*
MnO	0.07 *[0.00-0.16]*	0.05 *[0.00-0.17]*	0.03 *[0.00-0.13]*	0.03 *[0.00-0.20]*	3.84 *[2.56-5.36]*	2.12 *[0.00-6.36]*	0.55 *[0.41-0.71]*	0.43 *[0.01-1.08]*	2.13 *[0.92-2.92]*	1.19 *[0.84-1.53]*
MgO	38.99 *[37.39-40.20*	37.40 *[25.27-41.36]*	3.20 *[0.18-20.76]*	34.28 *[28.58-38.11]*	2.09 *[0.88-4.25]*	6.59 *[0.55-13.94]*	0.58 *[0.34-1.02]*	0.64 *[0.04-1.82]*	37.97 *[34.46-43.48]*	56.87 *[54.80-58.93]*
CaO	0.04 *[0.00-0.08]*	0.12 *[0.00-1.69]*	30.94 *[12.11-34.24]*	0.09 *[0.01-0.47]*	0.12 *[0.11-0.15]*	0.06 *[0.00-0.16]*	0.01 *[0.00-0.03]*	0.03 *[0.00-0.12]*	0.04 *[0.00-0.19]*	0.06 *[0.00-0.12]*
NiO	0.00 *[0.00-0.00]*	0.27 *[0.00-0.62]*	0.07 *[0.00-0.79]*	0.13 *[0.00-0.36]*	0.08 *[0.04-0.14]*	0.13 *0.00-0.48]*	0.26 *[0.22-0.33]*	0.11 *[0.02-0.25]*	0.16 *[0.00-0.42]*	0.14 *[0.00-0.28]*
	n=8	n=192	n=51	n=12	n=6	n=23	n=4	n=10	n=6	n=2

n- number of analyses; [a-b]- concentration range. * SEM-EDS (Energy Dispersive Spectroscopy) analyses.

Querceto serpentinite samples are characterized by typical pseudomorphic mesh texture (Fig. 5a, b). QU-2 sample is completely altered, and shows large veins of magnetite that cut the entire thin section (Fig. 5a). QU-3 samples contain Fe-rich brucite veins (Fig. 5b). Chromites are scarce and show similar alteration features (Fig. 5c, d) as Santa Luce primary spinels, described above. Locally, very small relicts of primary spinel (Mg-Al-chromites) have been observed. Noticeably, these relicts lie generally at the rims of the pseudomorphic texture replacing the primary spinel (Fig. 5c, d). In addition, Querceto serpentinites are characterized by a whitish coating of hydrated carbonates. SEM-EDS analyses revealed that the main carbonates are Mg-rich (i.e., hydromagnesite, nesquehonite, etc), with minor amount of the so-called "layered double hydroxide" family. The latter phases can be considered as mixed hydroxides of di- (e.g., Mg^{2+}, Ni^{2+}, Co^{2+}) and tri-valent (e.g., Cr^{3+}, Al^{3+}) metal ions with CO_3^{2-} groups intercalated between the layers for the restoration of charge neutrality (e.g., coalingite, pyroaurite, stichtite, etc).

Bulk rock compositions (major and minor elements) of the selected samples, reported in Table 3, follow the serpentinite oceanic field composition (Niu, 2004) and are comparable to the nearby Cecina Valley serpentinites (Mellini et al., 2005; Table 3) and to the unaltered serpentinites reported by Boschi et al. (2009). The Cr content of the rocks varies from ~3100 to 2500 ppm, Ni content from ~ 1900 to ~ 2600 ppm, within the average of the oceanic serpentinites.

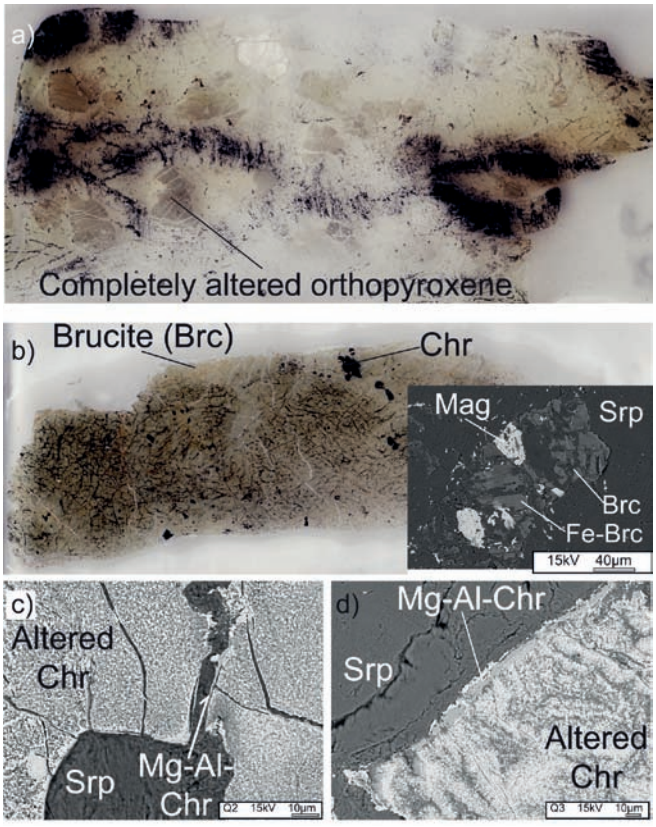

Fig. 5 - Petrographic features of serpentinite rock samples from Querceto. a) and b) Scan of thin sections showing main textural features and mineralogy of QU-2 and QU-3 samples, respectively. The inset in Fig. 5b) shows a FE-SEM BSE image of brucite. c) and d) FE-SEM BSE images of completely altered chromite showing only small relicts of primary Mg-Al-chromite.

Soil properties, petrography and bulk concentrations

Selected soils have the following common characteristics, summarized in Fig. 6: (I) dark colour at the top; (II) thin litter cover (O horizon); (III) high root density in the

A horizons, loamy to sandy loam texture with a few serpentinite stones in the B horizons; (IV) sandy clay loam texture with a high density of serpentinite relicts. Finally, soils are not deep and do not exceed a depth of 80 cm.

Each soil horizons, according to petrographic analyses of different fractions, are mainly composed by: i) rock fragments; ii) aggregates of minerals and rock fragments; iii) single mineral or association of a few minerals. Fragments of preserved rocks prevail within the > 0.50 mm and > 2 mm fractions of the whole pedon thickness. They show fabric similar to that of the rock samples taken from the bedrock. They can be either unaltered or so highly weathered preventing the mineral identification. Aggregates of rock fragments and/or minerals may be composed either of clasts with comparable dimensions or, more commonly, they consist of a large rock fragment with minor clasts of various composition. Clasts composed of highly resistant phases, such as Mg-Al-chromite, garnet and clinopyroxene, have been rarely observed within intermediate soil fractions (> 0.25 mm). Chromite from the soils shows the same petrographic features as those observed for the rocks samples (Fig. 7). Mg-Al-chromite occurs as unaltered (Fig. 7a, d), partially (Fig. 7b, e) and/or totally replaced by secondary spinels (i.e., chromite and/or magnetite) and/or fine-grained aggregates of phyllosilicates and oxides (Fig. 7c, f). Generally, magnetite occurs only at the external rims and/or within fractures, whereas the Fe-chromite growth occurs internally and also along fractures and discontinuous rims (Fig. 7d-f). Locally, small relicts of Mg-Al-chromite at the boundary between Fe-chromite and magnetite have been observed within the Querceto soil samples (Fig. 7f).

Major and minor elements of selected soil profiles are reported in Table 4. Besides Si, Mg is the predominant cation, followed by Fe and Al, whereas, trace metals consist mainly of Cr (up to 3196 ppm) and Ni (up to 3123 ppm). L.O.I. content increases substantially from serpentinite bedrocks to soils; in particular, SLS-1A horizon shows 21 wt% L.O.I. (average L.O.I. content of Santa Luce serpentinite = 12.9 wt%), whereas QUS-C (the deepest horizon) reach the highest L.O.I. content (15.9 wt%).

SiO_2 from both soils profiles shows the highest concentration within the B horizon (Fig. 6). The B and C SLS hori-

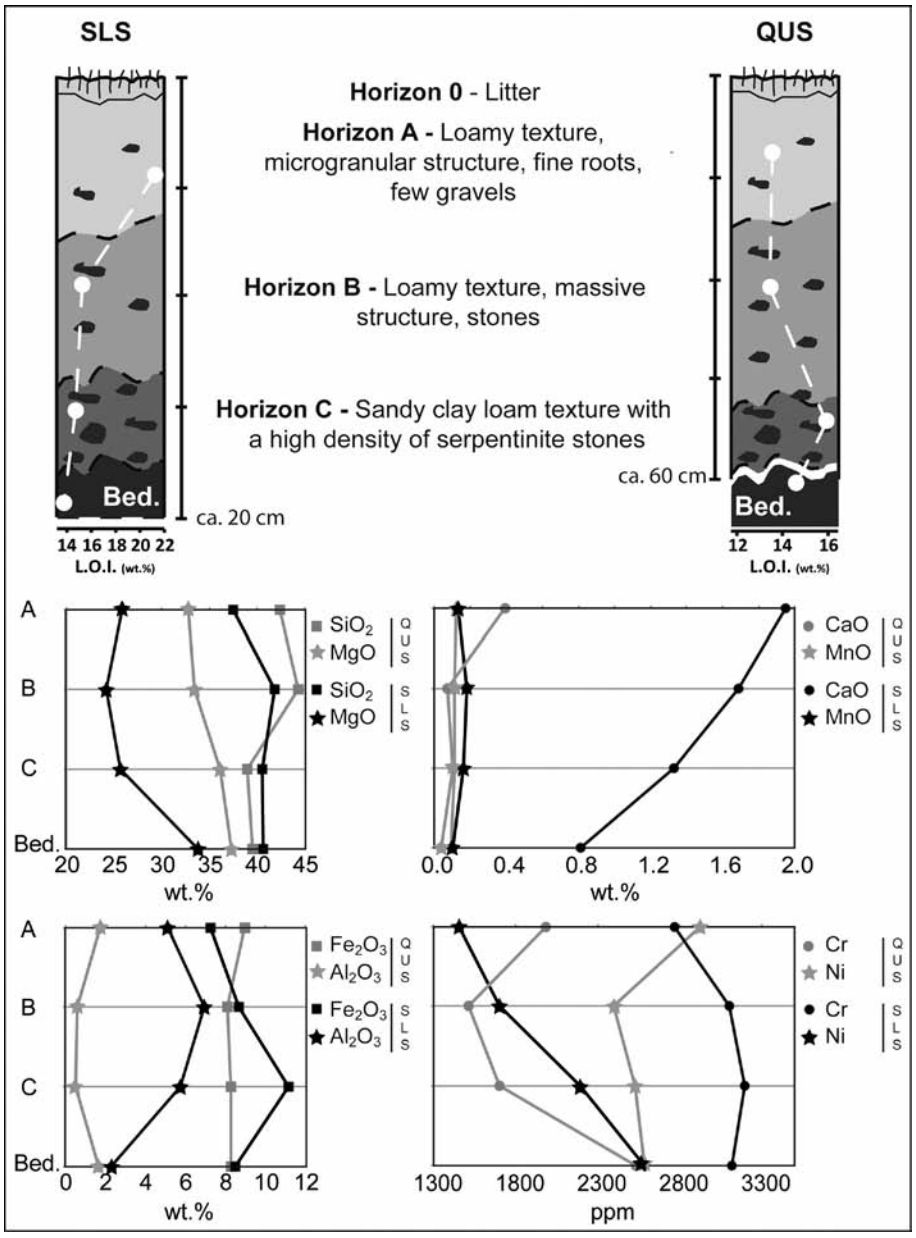

Fig. 6 - Sketch of soil profiles from Santa Luce (SLS) and Querceto (QUS) showing pedological properties and L.O.I. variations (wt.%, white dots) through the profiles. Chemical profiles of some major (SiO_2; MgO; CaO; MnO; Fe_2O_3; Al_2O_3) and trace (Cr; Ni) elements are also shown.

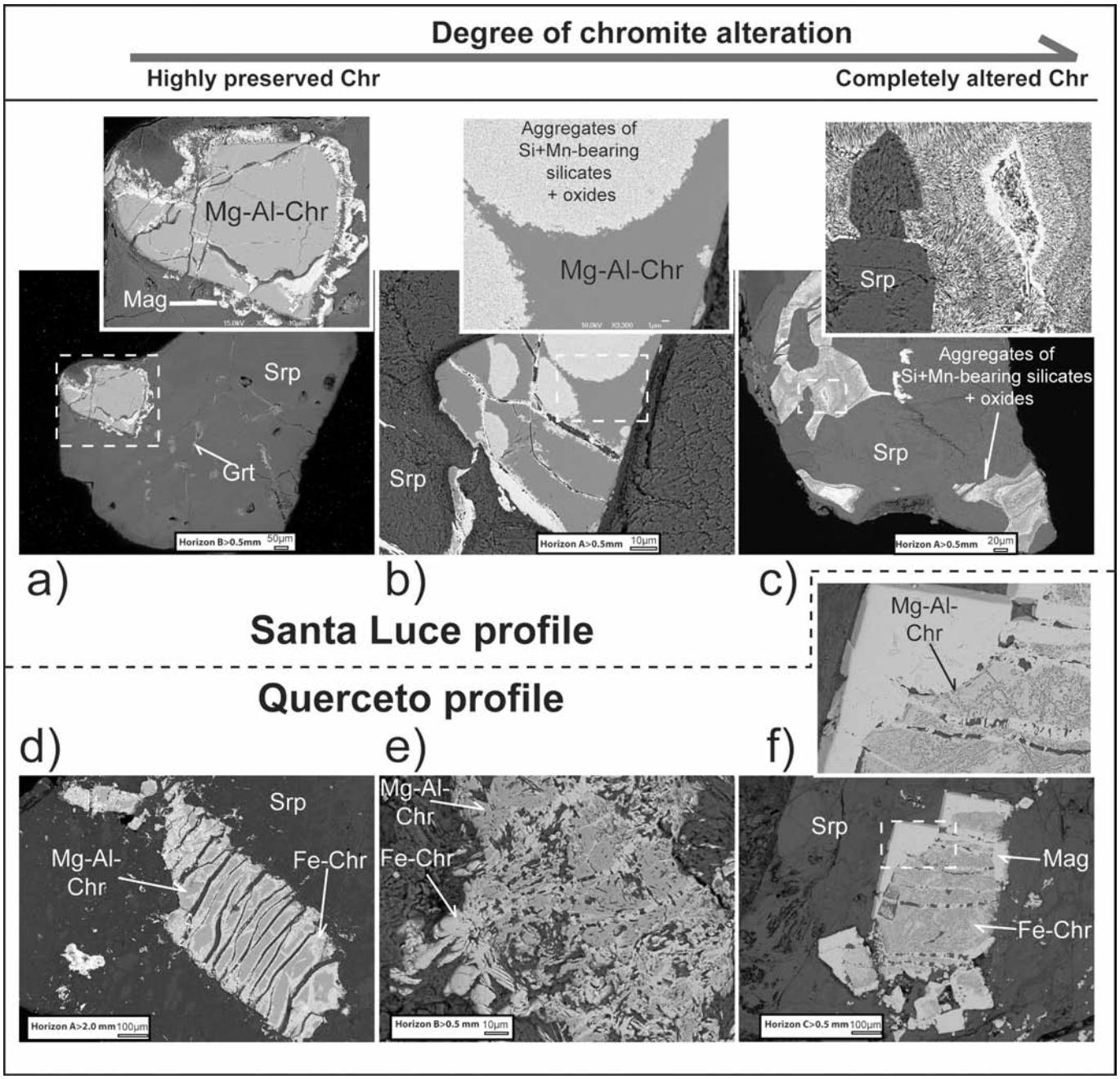

Fig. 7 - Alteration features of chromite from soil samples. FE-SEM BSE images showing the different degree of alteration of chromite from Santa Luce quarry [a), b), and c)], and Querceto [d), e), and f)].

zons are characterized by SiO_2 content comparable with that of the bedrock, whereas the A horizon is slightly depleted. Contrarily, the uppermost A and B horizons of the QUS profile show slightly higher SiO_2 content with respect to the C horizon and the bedrock.

The MgO wt% (Fig. 6) of the Querceto profile increases from the shallower to the deeper horizons and it is generally only slightly lower than the MgO wt% of rock samples. Contrarily, the soil horizons from the Santa Luce profile show a larger difference in terms of MgO wt% with respect to the MgO wt% of rocks and show the lowest values within the B horizon (24.21 wt%).

MnO within the soils profiles of both localities is generally low (below 0.3 wt%) and comparable to the MnO wt% of rock samples (Fig. 6).

The CaO wt% shows (Fig. 6) a gradual decrease from the A to the C horizon of the SLS profile (from 1.95 to 1.33 wt%), whereas, an abrupt variation, from 0.39 of the A-horizon to 0.07 and 0.10 wt% of the B and C horizons, respectively, characterises the CaO trend within the QUS profile. Noticeably, the CaO wt% of the Santa Luce soil profile is higher than the rock samples (0.81 wt%). The high CaO content of the bedrock directly below the soil profile of Santa Luce is due to the occurrence of secondary Ca-rich phases, such as hydrogarnet. Consequently, the high CaO values obtained from the different soil horizons are probably linked to the occurrence of hydrogarnet fragments and in part to the common presence of plagioclase fragments.

The Fe_2O_3 content of both soil profiles is comparable to that of the bedrocks (ca. 8 wt%) except for the C horizon of

the Santa Luce profile which results Fe_2O_3 enriched with respect to the bedrock (Fig. 6).

The Al_2O_3 wt% (Fig. 6) shows opposite trends for the two soil profiles. Within the Santa Luce profile the Al_2O_3 content is higher than the Al_2O_3 content of the bedrock and shows the highest concentration within the B horizon. The Al_2O_3 variation from soil horizons to the bedrock of the Querceto samples is less pronounced; here the B and C horizons are slightly depleted with respect to the bedrock.

Opposite trends have been obtained also for the distribution of Cr and Ni among the different soils horizons (Fig. 6). The SLS soil profile shows an increase of Cr, from 2765 to 3196 ppm, downward with the Cr content of the C horizon slightly higher than the Cr content of the bedrock. Ni varies from 1454 to 2192 ppm going from the A to the C horizon and generally is always significantly lower than the Ni content of the bedrock. The QUS profile is characterized by a decrease of Cr from the A to the B horizon and a subsequent increase from the B to the C horizon. Noticeably, the soil horizons of the QUS profile are depleted in Cr with respect to the bedrock. The Ni content of the B and C horizons is comparable with the Ni content of the bedrock. The soil horizon A show a very high Ni content, higher than the Ni content of the bedrock.

Summarizing, the SLS horizons are richer in Al_2O_3 and CaO and depleted in MgO wt% with respect to QUS horizons (Al_2O_3 > 5 wt% vs. < 2 wt%; CaO > 1.30 wt% vs < 0.4 wt%; MgO < 26 wt% vs > 32 wt%). Moreover, the Cr and Ni contents of the SLS soil horizons are, respectively, lower and higher than the soils horizons from the Querceto profile.

Mineral chemistry of rocks and soils

Representative chemical analyses of minerals observed both in rocks and soils samples from Santa Luce and Querceto are reported in Table 5 and Table 6, respectively. EMPA analyses from both soil and rock samples of the Santa Luce quarry show that chromium is very abundant within Mg-Al-chromites (23-41 wt% of Cr_2O_3), whereas, the Cr_2O_3 of magnetite and silicates is generally lower than 3 wt% (Fig. 8). Serpentine group minerals are generally chromium-free, except for serpentine bastite (Fig. 8). No systematic differences between minerals from soils and rocks have been detected. The Cr_2O_3 contents of Mg-Al-chromites from Querceto soil and rock samples ($23 < Cr_2O_3 < 45$ wt%) are comparable with those obtained from Mg-Al-chromites of the Santa Luce area, whereas, magnetite, serpentine and chlorite from the Querceto samples are richer in Cr with respect to the equivalent mineral phases of the Santa Luce quarry (Fig. 8).

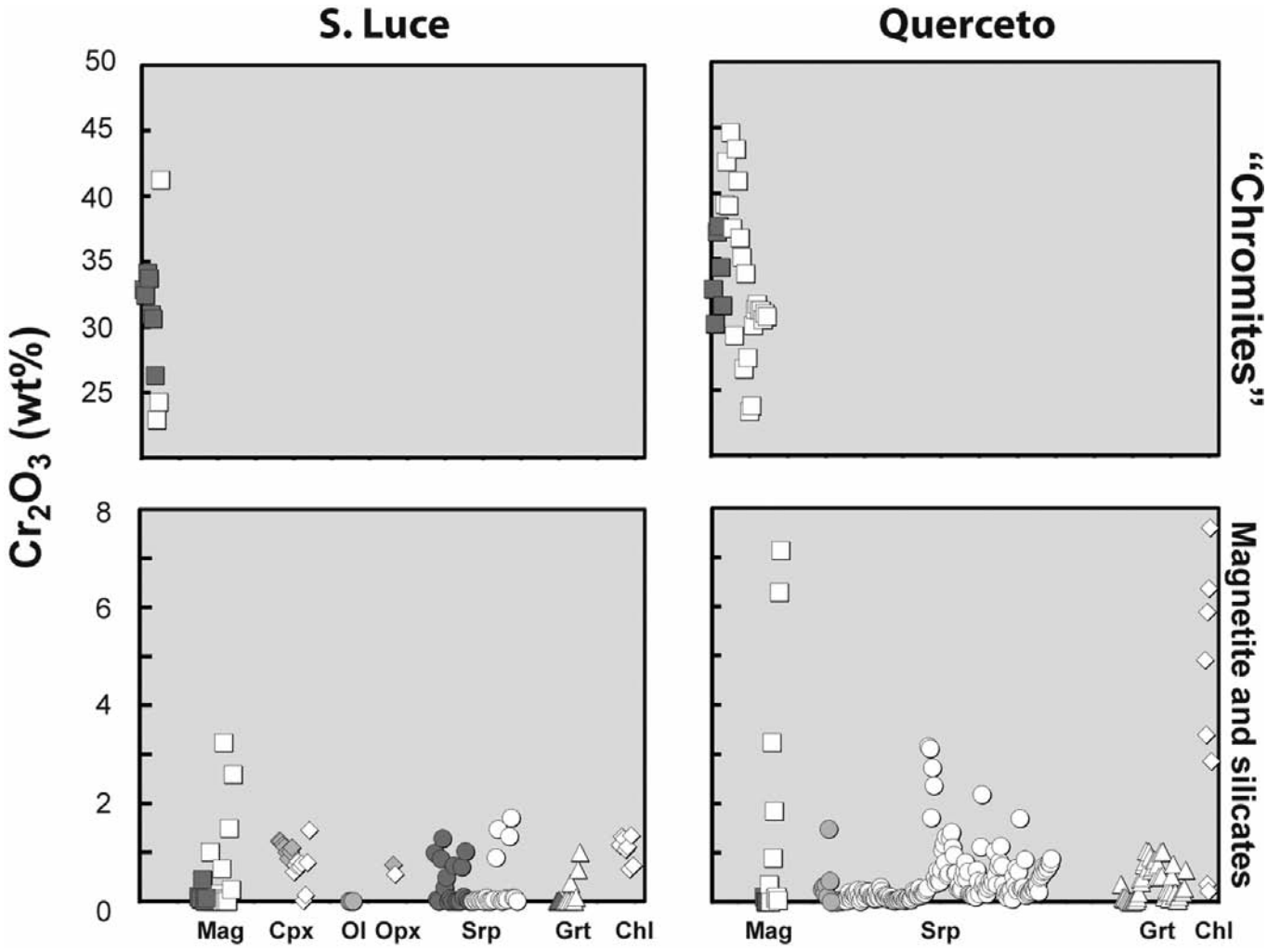

Fig. 8 - Cr_2O_3 content (wt.%; EMPA data) of minerals from rock and soil samples of Santa Luce and Querceto localities. Grey and white symbols refer to minerals analysed within rock and soils samples, respectively.

Also in this case, serpentine bastites are richer in chromium with respect to serpentines after olivine.

The MnO wt% of Mg-Al-chromites from the Santa Luce samples is very low except for a single value at about 7 wt% (Fig. 9). The MnO content of magnetite varies from 0.0 to 0.3 wt%, with one single value at 0.7 wt%, and is comparable to the MnO content of silicates. Noticeably, the MnO content of Mg-Al-chromites from Querceto samples is highly variable from 0.0 (Mg-Al-chromite) to about 7.0 wt% (Fe-chromites). Analogously, the MnO content of magnetite is higher than the MnO content of magnetite from Santa Luce quarry. Serpentine and garnet are near Mn-free, whereas chlorite contains up to 0.4 wt% of MnO (Fig. 9).

DISCUSSION

Comparison between the two case studies

The Cr-bearing waters from Querceto are enriched of Mg (Ca/Mg ranges from 0.01 to 0.18) with respect to those of Santa Luce, as showed in the Fig. 3c. Noticeably, the Querceto soil and rock samples are richer in MgO with respect to those from Santa Luce. Brucite has been observed only within the Querceto rock samples suggesting a possible correlation between its occurrence and the higher MgO content of soil, rock and water samples. The occurrence of brucite within partially serpentinized Alpine-type ultramafic rocks from the circum-Pacific orogenic belts has been attributed by Hostetler et al. (1966) to a pervasive serpentinization of dunites and high-olivine peridotite. The authors have also noted that in areas of intense shearing or fracturing brucite does not occur. According to Frost and Beard (2007) the assemblage serpentine + brucite marks the lowest silica activity reached in most serpentinites. The presence and distribution of brucite, which commonly is a cryptic phase in serpentinites, may provide key information about the scale over which silica activity varied within a serpentinite, and this will provide important clues to the process by which serpentinization occurred. Moreover, the distribution of brucite in a rock is important because it may provide evidence of fluid pathways that operated during serpentinization and may indicate the direction of fluid flow. According to Frost and Beard (2007) fluids that are moving upwards from a serpentinization front should have low silica activity and their pathways should be marked by the presence of abundant brucite. The absence of brucite within the Santa Luce samples may be explained by the following three reasons: i) a different protolith (i.e., olivine-poor) with respect to the Querceto sample; ii) a different degree of deformation (i.e., shearing or fracturing); iii) a difference in fluid pathways. According to

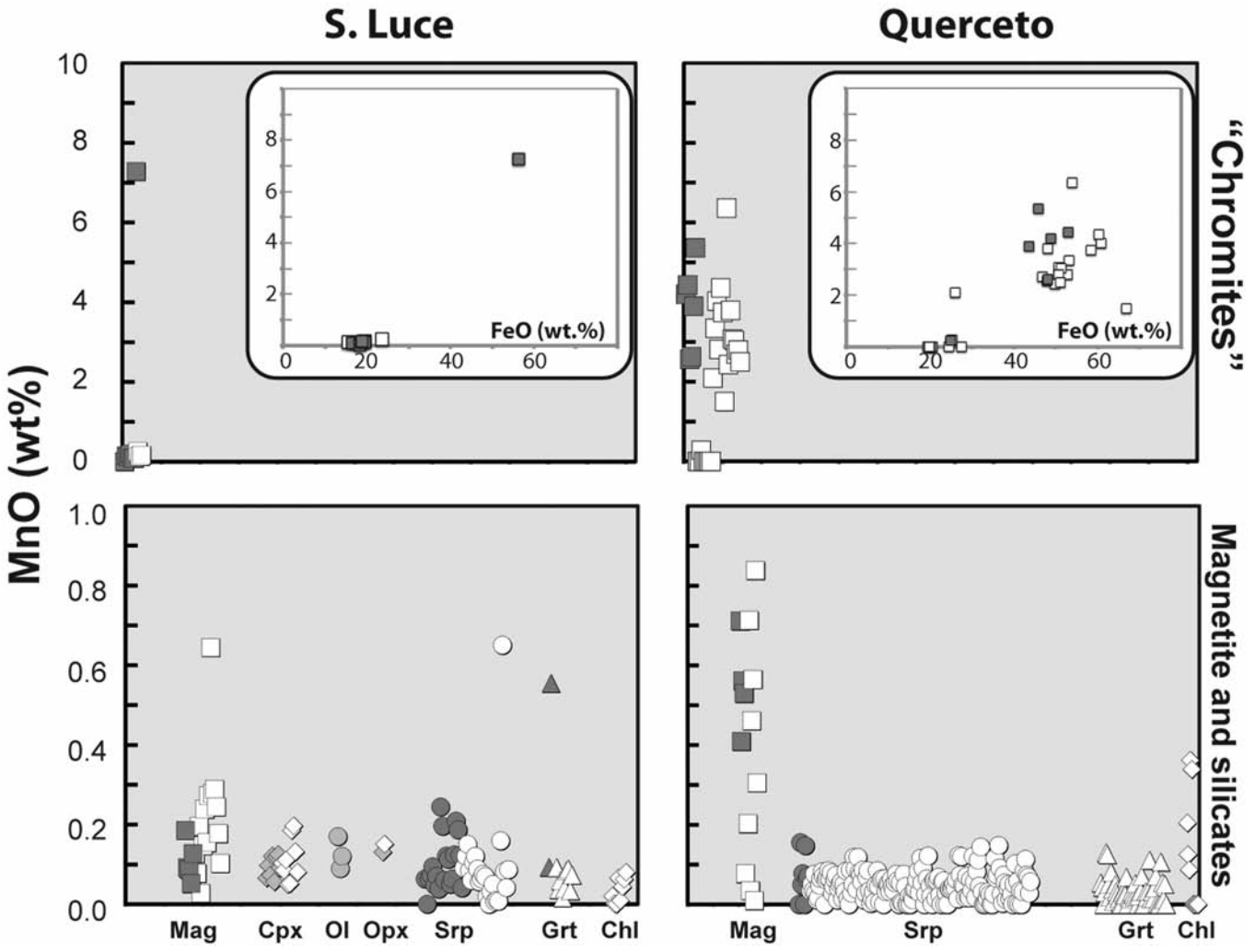

Fig. 9 - MnO content (wt%; EMPA data) of minerals from rock and soil samples of Santa Luce and Querceto localities. The FeO (wt%; EMPA data) of chromites is also shown. Grey and white symbols refer to minerals analysed within rock and soils samples, respectively.

the petrographic and chemical analyses, the protholits of serpentinitic samples from both localities are similar. Therefore, the absence of brucite within the Santa Luce samples is more easily explainable as consequence of different degree of fracturing and/or of different silica activity mainly controlled by fluid pathways.

The Santa Luce serpentinites show lower values of MgO wt% and higher SiO_2 wt% compared to the Querceto bedrocks, as well as compared to average serpentinites values (Niu, 2004). These evidences could suggest that Santa Luce serpentinite outcrop underwent a pervasive Si-rich metasomatism, as already reported in many Tuscan serpentinites outcrops (Boschi et al., 2009). Alternatively, the low MgO/SiO_2 ratios could be due to the dissolution at low temperature (< 150°C) of brucite formed during serpentinization, as already reported by Snow and Dick (1995). By contrast, the localized clay-rich alteration, observed at Querceto, show similar high SiO_2 content but higher MgO/SiO_2 ratio and lower Al_2O_3 and Cr contents, most probably related to low temperature weathering. The Santa Luce rock and soil samples show a relatively higher CaO concentration with respect to those of the Querceto locality. As well as CaO, the Santa Luce soil horizons show a higher Al_2O_3 content with respect to both its own bedrock and to the Querceto soil and rock samples. The Santa Luce serpentinitic body is cut by plagiogranite dykes and, within the soil samples, plagioclase is common. Therefore, the Al_2O_3 and CaO contents of soils from Santa Luce are mainly controlled by both Ca-rich phases related to metasomatic events (i.e., hydrogarnet) and by mineral phases deriving from the weathering of felsic rocks. The latter suggests a lateral transport during pedogenesis.

Trace elements soil profiles show that the Cr content of both rock and soil samples from Querceto is lower than that of the Santa Luce samples. Moreover, the Cr content of the Querceto soil horizons is depleted in Cr with respect to its own bedrock. It is interesting to note that only the QUW 1 water samples from Querceto are Cr(VI) rich, thus implying leaching processes of Cr(VI).

Cr distribution: from primary spinels to alteration products

Petrographic and chemical analyses have been focused mainly on Cr-bearing minerals with particular interest to the Cr-spinels and their alteration products. In both case studies, two main alteration features of primary Mg-Al-chromite have been recognised: replacement by fine-grained aggregates of oxides and silicates, locally with a concentric texture, and/or replacement by nearly homogeneous Fe-chromite. Rims of magnetite are commonly observed. Locally, the Fe-chromite domains are characterized by the occurrence of very small pores. A porous texture has been already described for the chromites of serpentinites from the Cecina Valley, in Tuscany, by Mellini et al. (2005). TEM observations led Mellini et al. (2005) to conclude that Fe-chromite consists of intergrowths of Cr-magnetite and silicates (intermixed lizardite and chlorite layers). We therefore suggest that the observed replacement textures consisting of fine-grained aggregates of silicates and oxides represent an evolved stage of the porous textures described by Mellini et al. (2005).

The alteration of primary spinels may occur during (e.g., Burkhard, 1993) or after the oceanic serpentinization (e.g., Mellini et al., 2005). Several features in favour to an alteration process coeval to the serpentinization have been observed. Mg-Al-chromite and the secondary spinel (i.e., Fe-chromite) may contain small amounts of SiO_2. Since Si does not go into the crystal structure of spinel, the detection of SiO_2 in chromites suggest the presence of a sub-microscopic silicate phases developed during serpentinization (Burkhard, 1993). According to Putnis and Austrheim (2010), during serpentinization of orthopyroxene silica-rich fluids may be generated if volume does not change. The occurrence of undisturbed orthopyroxene and clinopyroxene exsolved intergrowths is a demonstration of serpentinization under isovolumetric conditions (Viti et al., 2005). Noticeably, these features have been observed within the studied samples. Generally, the alteration of primary Mg-Al-chromite to Fe-chromite is also characterized by an increase of MnO, which may abruptly decrease within the outermost magnetite rim. Some interesting features on the correlation among elements during spinel alteration is clearly described by the Principal Component Analysis (PCA) of 6 elements (Al, Mg, Cr, Fe, Mn and O) analysed within the spinels (167 data) from Querceto site (Fig. 10). Chemical correlations are mainly described by two components (99.17%), the component 1 (F1) and 2 (F2). The F1 represents the inverse correlation between Fe and the other elements, in other words, it describes the subdivision between

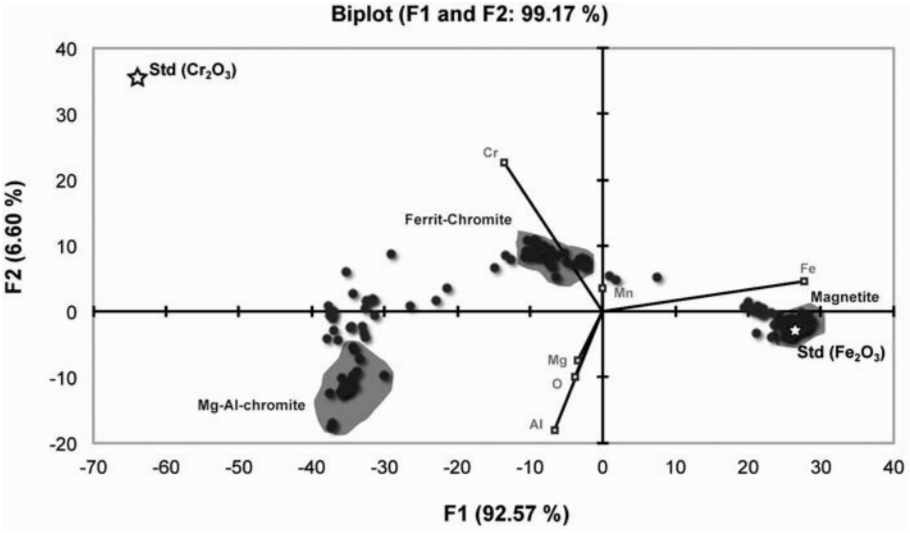

Fig. 10 - Principal Component Analysis of EMP data (167), of Mg-Al-chromite, Fe-chromite and magnetite from Querceto showing the correlation among six elements (Al, Mg, Cr, Fe, Mn and O). Analyses of pure Cr_2O_3 and Fe_2O_3 standards are also shown.

magnetite and chromite (Fig. 10). The F2 component describes the inverse correlation between Cr and Mn, with positive F2 coordinates, and Mg, O and Al, with negative F2 coordinates. The chemical information associated to this component allows confirming the existence of two types of chromite: the Mg-Al-chromite (Mn-free), and the Fe-chromites (Fe-rich and Mn-bearing; Fig. 10). This component describes the Mg-Al-chromite replacement by Fe-chromite already reported in Tuscany (e.g., Mellini et al., 2005) and elsewhere (e.g., Kimball, 1990). Noticeably, this reaction is accompanied by Mn enrichment of Fe-chromite. Different authors suggest the Mn enrichment is entirely secondary in origin, associated with low-temperature serpentinization and/or alteration (Paraskevopoulos and Economou, 1981; Gahlan and Arai, 2007; Grieco and Merlini, 2012). Alternatively, the decomposition of olivine during serpentinization could be the source of Mn, in a divalent oxidation state, which is released to hydrothermal solution (Singh and Singh, 2012). This process is potentially able to promote the oxidation of Mn before the interaction with spinels (e.g., Ivarsson et al., 2011).

As mentioned above, alteration of primary spinels may occur after the oceanic serpentinization. Mellini et al. (2005) reported the common occurrence of chloritic aureoles, up to 3 mm in size, around Fe-chromite rims and overgrowing mesh textures. Similar features were previously reported also by Gianfagna et al. (1992) for the Elba serpentinites. Mellini et al. (2005) concluded that the primary spinel alteration, the Fe-chromite formation and the wide chlorite reaction aureole formed after the oceanic serpentinization. Our samples lack of the metamorphic textures described by Mellini et al. (2005) and chlorite has been rarely observed, allowing us to exclude an important post-serpentinization re-equilibration of the primary spinel.

In summary, both the chemistry and texture of the primary spinel alteration products of studied samples are more compatible with a metasomatic process during oceanic serpentinization.

Origin of the Cr(VI): the possible role of Mn-oxides and hydroxyl-carbonates

Evidence for Cr(III) to Cr(VI) oxidation by Mn-oxides in natural systems have been reported by Fandeur et al. (2009b). These authors demonstrated by bulk XANES analyses the occurrence of Cr(VI) (up to 20 wt% of total chromium) in the unit of a regolith which is also enriched in Mn (MnO up to 21.7 wt%) due to the occurrence of Mn-oxides (identified as a mixture of asbolane, lithiophorite and birnessite). According to Fandeur et al. (2009b), Cr(VI) is associated with both Mn- and Fe-oxides, and especially at the boundary between these two oxides. Such a distribution of Cr(VI) suggests a possible reabsorption of Cr(VI) onto surrounding Fe-oxyhydroxides (mainly goethite) after oxidation by the Mn(IV)-oxides. The case study of Fandeur et al. (2009b) refers to ultramafic rocks that experienced a deep weathering under tropical conditions leading to the development of a lateritic regolith. Under Mediterranean climate, the conditions of the ophiolites weathering are completely different and in our study areas soil profiles are poorly developed, due to the combined effect of climate and geomorphology (e.g., De Siena and Vaselli, 1994). In addition, Mn-oxides are lacking from our rock and soil samples. A direct role of the Mn-oxides for the oxidizing Cr(III) to Cr(VI) reaction is thus difficult to demonstrate. Nonetheless, the oxidation of Cr(III) to Cr(VI) by Mn(VI)-oxides may occur at a very small scale between the different spinel types. In particular, the close association of very rich Cr-spinels (i.e., Mg-Al-chromite) with Mn-bearing spinels (i.e., Fe-chromite) and Fe dominated spinels (i.e., magnetite) may be compared to the textures observed by Fandeur et al. (2009b). High resolution in situ analyses, such as XANES spectroscopy, are needed in order to demonstrate this hypothesis. However, the potentially oxidizing mineral assemblage developed largely before (My) serpentinites become involved within the Critical Zone, resulting not the primary process for the environmental availability of Cr(VI). Consequently, the Cr(III) to Cr(VI) oxidation via other electrons acceptors is a more likely process in order to explain the Cr(VI) occurrence within waters under environmental conditions.

Fe-rich brucite, as recovered in Querceto samples (Fig. 5, Table 6), could be easily dissolved during serpentinites weathering (Mumpton and Thompson, 1965), producing a new mineral assemblage including hydrous magnesium carbonates and Mg-rich layered double hydroxides. During this process, ferrous iron in brucite is oxidized to ferric iron in layered double hydroxides. It is worth to note that some members of the layered double hydroxide group containing Ni^{2+} and Cr^{3+} behave as an electrochemical cell promoting the oxidative leaching of Cr^{3+} in the form of the soluble CrO_4^{2-} ion (hexavalent chromium; Radha and Kamath, 2004). Clear evidences for the ongoing dissolution of Fe-rich brucite at Querceto are the veinlets and crusts of hydrated Mg-rich carbonate (with minor amount of layered double hydroxides) covering and crosscutting serpentinite both inside and outside the drainage tunnel, where the Cr(VI)-rich spring water was sampled (Boschi et al., 2012). The whole process is summarized in Fig. 11. Similarly, in other Tuscan localities, Cr(VI)-bearing waters have been collected (Baneschi et al., 2011) in association with brucite-rich serpentinites and hydrated Mg-carbonate precipitates (e.g., Boschi et al., 2011).

In summary, multiple parameters could drive the local occurrence of Cr(VI)-bearing spring waters. Small local

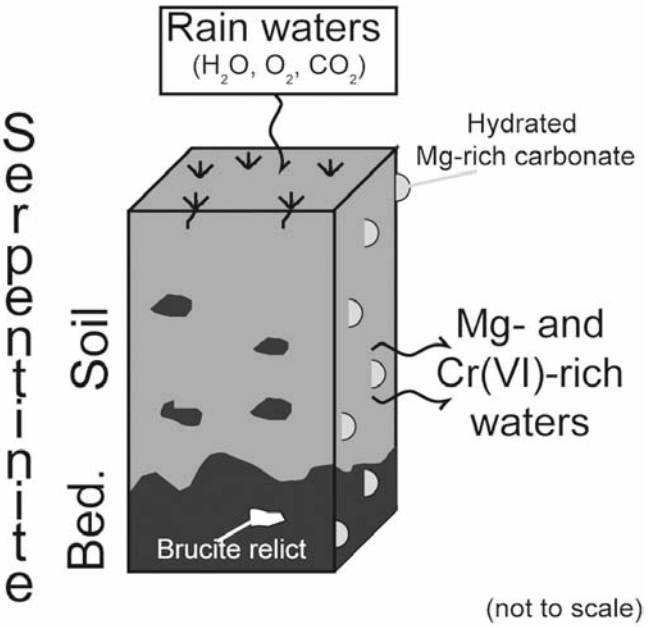

Fig. 11 - Scheme summarizing the observed features at Querceto: the Fe-brucite oxidation, the hydrated Mg-rich carbonate precipitation and the Cr(III) to Cr(VI) oxidation.

climate variations, different geological features of the aquifers (i.e., protoliths, degree of serpentinization, fluids pathways during serpentinization), interaction with the organic matter and different pathways of the ground waters may concur for the observed local occurrence of Cr(VI)-bearing spring waters. Our first investigation highlighted the possible correlation between brucite-rich serpentinites, hydrated Mg-rich carbonates + layered double hydroxides precipitation and Cr(VI)-bearing waters. Further detailed geological, petrological and mineralogical studies of these processes could help the understanding the processes of oxidation and release of Cr(VI) in the groundwater/spring waters in ophiolitic formations.

CONCLUSIONS

Our results show that Cr(VI)-bearing spring waters occur only at Querceto where Fe-brucite-rich serpentinites are coated by a whitish precipitation of hydrated Mg-rich carbonates. Here, both rock and soil samples are characterized by a lower Cr concentration with respect to the samples from the Santa Luce quarry where spring waters are Cr(VI)-free.

The alteration of primary Mg-Al-chromite within rock and soil samples from both localities is mainly characterized by a replacement of secondary spinels and/or fine-grained aggregates of oxides and silicate (e.g., serpentine and chlorite). These secondary phases show an enrichment of MnO as consequence of metasomatic events. The co-occurrence of Mn-bearing Fe-chromite, magnetite and unaltered chromite could be responsible for the local Cr(III) to Cr(VI) oxidation. This represent, at local scale, the process reported by Fandeur et al. (2009b) for deep weathered ultramafic rocks under tropical conditions. However, the observed mineral assemblages (ubiquitous in both the study localities) formed before the superficial exposure of the rocks, i.e., during oceanic serpentinization, and could not be associated to the ongoing release of Cr(VI) into the spring waters. In addition, Mediterranean climate conditions prevent the Mn-oxides formation within soils during pedogenetic processes.

Finally, our study highlighted the correlation between brucite dissolution, hydrated Mg-carbonates precipitation and Cr(VI)-rich spring water, suggesting that Cr(III) to Cr(VI) oxidation under Mediterranean climate conditions may be more realistically related to other processes involving different electrons acceptors and, more likely, complex mineral phases (layered double hydroxides, hydroxy-carbonates, etc.) that still need to be investigated.

ACKNOWLEDGMENTS

The authors thank M. Fialin and F. Couffignal from the Centre de Microanalyses CAMPARIS (University Pierre et Marie Curie, Paris, France) for their help during EPMA analyses. We would like to thank the Italian Society of Mineralogy and Petrology (SIMP) for its contribution (grant) for scientific collaborations with foreign colleagues. In particular, we would like to thank Dr. Gaston Godard and the whole IPGP for the kindly welcome and for the very helpful collaboration. This research is partially supported by RESPIRA project (POR-FSE 2007-2013; Regione Toscana - EU).

Encouragements by Editors and constructive reviews by L. Gaggero and G. Bianchini are gratefully acknowledged.

REFERENCES

Ball J.W. and McCleskey R.B., 2003. A new cation-exchange method for accurate field speciation of hexavalent chromium. Talanta, 61: 305-313.

Baneschi I., Langone A., Boschi C., Agostini S., Dallai L., Dini A., Guidi M. and Tonarini S., 2011. Chromium (III) and Chromium (VI) in serpentinites spring waters in Tuscany (Italy). Epitome.04.0344. Geoitalia 2011.

Boschi C., Baneschi I., Langone A., Agostini S., Dallai L., Dini A., Guidi M. and Tonarini S., 2011. Spontaneous CO_2 mineralogical sequestration in mine waste materials: an example from Montecastelli copper mine (Tuscany). Epitome.04.0357.Geoitalia2011.

Boschi C., Dallai L., Dini A., Baneschi I., Langone A., Cavallo A. and Ruggieri G., 2012. The carbon dioxide mineral sequestration analogues: examples from Tuscany (Italy). Goldschmidt 2012 Abstr.

Boschi C., Dini A., Dallai L., Ruggieri G. and Gianelli G., 2009. Enhanced CO_2-mineral sequestration by cyclic hydraulic fracturing and Si-rich fluid infiltration into serpentinites at Malentrata (Tuscany, Italy). Chem. Geol., 265: 209-226.

Bruni J., Canepa M., Cipolli F., Marini L., Ottonello G., Vetuschi Zuccolini M., Chiodini G., Cioni R. and Longinelli A., 2002. Irreversible water-rock mass transfer accompanying the generation of the neutral, Mg-HCO_3 and high-pH, Ca-OH spring waters of the Genova province, Italy. Appl. Geochem., 17: 455-474.

Burkhard D.J.M., 1993. Accessory chromium spinels: Their coexistence and alteration in serpentinites. Geochim. Cosmochem. Acta, 57: 1297-1306.

Caillaud J., Proust D., Philippe S., Fontaine C. and Fialin M., 2009. Trace metal distribution from a serpentine weathering at the scale of the weathering profile and its related weathering microsystems and clay minerals. Geoderma, 149: 199-208.

Chiarucci A., Bovini I. and Fattorini L. 2003. Community dynamics of serpentine vegetation in relation to nutrient addition and climatic variability. J. Medit. Ecol., 4: 23-30

Chiarucci A., Foggi B. and Selvi E. 1995. Garigue plant communities of ultramafic outcrops of Tuscany (Italy). Webbia, 49: 179-192.

Cipolli F., Gambardella B., Marini L., Ottonello G. and Vetuschi Zuccolini M., 2004. Geochemistry of high-pH waters from serpentinites of the Gruppo di Voltri (Genova, Italy) and reaction path modeling of CO_2 sequestration in serpentinite aquifers. Appl. Geochem., 19: 787-802.

De Siena C. and Vaselli O., 1994. Pedological, mineralogical and geochemical investigations of ophiolitic soils from the Lanciaia-Montecastelli Pisano (Tuscany, Italy). Mem. Soc Geol It., 48: 675-680.

Elter P., 1975. L'ensemble ligure. Bull. Soc. Géol. Fr., 17: 984-997.

Fandeur D., Juillot F., Morin G., Olivi L., Cognigni A., Ambrosi J-P., Guyot F. and Fritsch E., 2009a. Synchrotron-based speciation of chromium in an Oxisol from New Caledonia: Importance of secondary Fe-oxyhydroxides. Am. Mineral., 94: 710-719.

Fandeur D., Juillot F., Morin G., Olivi L., Cognigni A., Webb S.M., Ambrosi J-P., Fritsch E., Guyot F. and Brown G.E. Jr., 2009b. XANES evidence for exidation of Cr(III) to Cr(VI) by Mn-oxides in a lateritic regolith developed on serpentinized ultramafic rocks of New Caledonia. Environ. Sci. Technol., 43: 7384-7390.

Fantoni D., Brozzo G., Canepa M., Cipolli F., Marini L., Ottonello G. and Vetuschi Zuccolini M., 2002. Natural hexavalent chromium in groundwaters interacting with ophiolitic rocks. Environ. Geol. 42: 871-882.

F.A.O., 1998. World reference base for soil resources. World Soil Resources Reports 84, Rome.

Fendorf S.E., 1995. Surface reactions of chromium in soils and waters. Geoderma, 67: 55-71.

Franzini M., Leoni L. and Saitta M., 1975. Revisione di una metodologia analitica per fluorescenza-X, basata sulla correzione completa degli effetti di matrice. Rend. Soc. Ital. Mineral. Petrol., 31: 365-378.

Frost B.R. and Beard J.S., 2007. On silica activity and serpentinization. J. Petrol., 48: 1351-1368.

Gahlan H.A. and Arai S., 2007. Genesis of peculiarly zoned Co, Zn, Mn-rich chromiam spinel in serpentinite of Bou-Azzer ophiolite, Anti-Atlas, Morocco. J. Mineral. Petrol. Sci., 102: 69-85.

Garnier J., Quantin C., Guimarães E. and Becquer T., 2008. Can chromite weathering be a source of Cr in soils? Mineral. Mag., 72: 49-53.

Garnier J., Quantin C., Martins E.S. and Becquer T., 2006. Solid speciation and availability of chromium in ultramafic soils from Niquelândia, Brazil. J. Geochem. Explor., 88: 206-209.

Garrels R.M., 1968. Genesis of some ground waters from igneous rocks. In: Abelson P.H. (Ed.), Researches in geochemistry, Wiley, 2: 406-420.

Gasser U.G., Juchler S.J., Hobson W.A. and Sticher H., 1995. The fate of chromium and nichel in subalpine soils derived from serpentinite. Can. J. Soil Sci., 75: 187-195.

Gianfagna A., Grubessi O. and Massera S., 1992. Cr-rich-spinel chemistry of the serpentinites from the island of Elba, Tuscany, Italy: note I. Atti Soc. Tosc. Sci. Nat. Mem., 99: 175-194.

Grassi S., 2009. Origine del cromo esavalente in Val di Cecina e valutazione integrata degli effetti ambientali e sanitari indotti dalla sua presenza - Rapporto conclusivo della prima fase del progetto IGG-CNR, ISE-CNR, ARPAT.

Grieco G. and Mellini A., 2012. Chromite alteration processes within Vourinos ophiolites. Int. J. Earth Sci., 101:1523-1533.

Hostetler P.B., Coleman R.G. and Mumpton F.A., 1966. Brucite in alpine serpentinites. Am. Mineral. 51: 75-98.

Ivarsson M., Broman C. and Holm N.G., 2011. Chromite oxidation by manganese oxides in subseafloor basalts and the presence of putative fossilized microorganisms. Geochem. Trans., 12: 5

Kimball K.L., 1990. Effects of hydrothermal alteration on the composition of chromian spinels. Contrib. Mineral. Petrol., 105: 337-346.

Koppen W. 1936. Das geographisca System der Klimate. In W. Koppen and G. Geiger (Eds.), Handbuch der Klimatologie, C. Gebr, Borntraeger, 1: 1-44.

Leoni L. and Saitta M., 1976. X-ray fluorescence analysis of 29 trace elements in rock and mineral standards. Rend. Soc. It. Miner. Petrol., 32: 497-510.

Marchetto A., Arisci S., Buffoni A., Giacometti P., Orrù A., Mangoni M., Manini C., Pranzo A., Rogora M., Tartari G.A. and Tornimbeni O., 2012. La chimica delle deposizioni atmosferiche e gli inquinanti atmosferici nelle aree del programma CONECOFOR nell'anno 2011. Report CNR-ISE, 02.12: 23 pp.

Margiotta S., Mongelli G., Summa V., Paternoster M. and Fiore S., 2012. Trace element distribution and Cr(VI) speciation in Ca-HCO_3 and Mg-HCO_3 spring waters from the northern sector of the Pollino massif, southern Italy. J. Geochem. Explor.: 115: 1-12.

Marroni M. and Pandolfi L., 1996. The deformation history of an accreted ophiolite sequence: the Internal Liguride units (Northern Apennines, Italy). Geodin. Acta, 9 (1): 13-29.

Marroni M., Della Croce G. and Meccheri M., 1988. Structural evolution of the Mt. Gottero Unit in the Mt. Zatta-Mt. Ghiffi sector (Ligurian-Emilian Apennines). Ofioliti 13: 29-42.

Mellini M., Rumori C. and Viti C., 2005. Hydrothermally reset magmatic spinels in retrograde serpentinites: formation of ''ferritchromit'' rims and chlorite aureoles. Contrib. Mineral. Petrol., 149: 266-275.

Molli G., 2008. Northern Apennine-Corsica orogenic system: an updated overview. In: S. Siegesmund, B. Fügenschuh and N. Froitzheim (Eds), Tectonic aspect of the Alpine-Dinaride-Carpathian System. Geol. Soc London Spec. Publ., 298: 413-422.

Moraetis D., Nikolaidis N.P., Karatzas G.P., Dokou Z., Kalogerakis N., Winkel L.H.E. and Palaiogianni-Bellou A., 2012. Origin and mobility of hexavalent chromium in North-Eastern Attica, Greece. Appl. Geochem., 27: 1170-1178.

Mumpton F.A. and Thompson C.S., 1965. The stability of brucite in the weathering zone of the New Idria serpentinite. Clays Clay Min., 14: 249-257.

Nirta G., Pandeli E., Principi G., Bertini G. and Cipriani N., 2005. The Ligurian Units of Southern Tuscany. Boll. Soc. Geol. It., spec. vol., 3: 29-54.

Niu Y., 2004. Bulk-rock major and trace element compositions of abyssal peridotites: Implications for mantle melting, melt extraction and post-melting processes deneath mid-ocean ridges. J. Petrol., 45: 2423-2458.

NRC (National Research Council), 2001. Basic research opportunities in Earth sciences. National Acad. Press, Washington, 154 pp.

Oze C., Bird D. and Fendorf S., 2007. Genesis of hexavalent chromium from natural sources in soil and groundwater. Proceed. Nat. Acad. Sci., 104: 6544-6549.

Oze C., Fendorf S., Bird D. and Coleman, R.G., 2004b. Chromium geochemistry of serpentine soils. International Geology Review, 46: 97–126.

Oze C., Fendorf S., Dennis K.B. and Coleman R.G., 2004a. Chromium geochemistry in serpentinized ultramafic rocks and serpentine soils from the Franciscan complex of California. Am. J. Sci., 304: 67-101.

Paraskevopoulos G.M. and Economou M., 1981. Zoned Mn-rich chromite from podiform type chromite ore in serpentinites of northern Greece. Am. Mineral., 66: 1013-1019.

Perugi A., Gabellini A. and Acciai A., 1995. Bosco di S. Luce. Carta naturalistica e escursionistica. SELCA Ed., Firenze.

Putnis A. and Austrheim H., 2010. Fluid-induced processes: metasomatism and metamorphism. Geofluids, 10: 254-269.

Radha A.V. and Kamath P., 2004. Oxidative leaching of chromium from layered double hydroxides: Mechanistic studies. Bull. Mater. Sci., 27: 355-360.

Singh A.K. and Singh R., 2012. Genetic implications of Zn- and Mn-rich Cr-spinel in serpentinites of the Tidding Suture Zone, eastern Himalaya, NE India. Geol. J. (DOI:10.1002/gj.2428).

Snow J.E. and Dick H.J.B., 1995. Pervasive magnesium loss by marine weathering of peridotite. Geochim. Cosmochim. Acta, 59: 4219-4235

Soil Survey Staff., 2003. Keys to Soil Taxonomy, 9th ed. USDA-Natural Resources Conservation Service, Washington, DC.

Visual MINTEQ ver 2.32. Stockholm Royal Institute of Technology (KTH), Stockholm.

Viti C., Mellini M. and Rumori C., 2005. Exsolution and hydration of pyroxenes from partially serpentinised harzburgites. Mineral. Mag., 69: 491-507.

Whitney D.L. and Evans B.W., 2012. Abbreviations for names of rock-forming minerals. Am. Mineral., 95: 185-187.

Received, November 12, 2012
Accepted, March 7, 2013